

1 **Does deep non-volcanic tremor occur in the central-eastern Mediterranean basin?**

2

3 **G. M., Bocchini<sup>1</sup>, P., Martínez-Garzón<sup>2</sup>, R. M., Harrington<sup>1</sup>, and M., Bohnhoff<sup>2,3</sup>**

4 <sup>1</sup>Faculty of Geosciences, Institute of Geology, Mineralogy, and Geophysics, Ruhr University  
5 Bochum, Bochum, Germany

6 <sup>2</sup>Helmholtz Centre Potsdam GFZ German Research Centre for Geosciences, Section 4.2  
7 Geomechanics and Scientific Drilling, Potsdam, Germany

8 <sup>3</sup>Institute of Geological Sciences, Free University of Berlin, Berlin, Germany.

9

10 †Corresponding author: Gian Maria Bocchini (gian.bocchini@rub.de), Faculty of Geosciences,  
11 Institute of Geology, Mineralogy, and Geophysics, Ruhr University Bochum, IA 4/135  
12 Universitätsstr. 150, 44801 Bochum (Germany).

13

14 **Key Points:**

- 15
- 16 • There is no unambiguous evidence for the occurrence of deep non-volcanic tremor in the  
central-eastern Mediterranean basin.
  - 17 • The thermal structure of subduction zones has an important control on deep tremorgenic  
18 conditions.
  - 19 • Very special physical conditions are required for deep tremorgenesis in settings that are  
20 not warm subduction zones.
- 21

## 22 **Abstract**

23 Non-volcanic tremor has been observed at the roots of many fault systems around the Pacific  
24 rim, including convergent and transform plate boundaries. The extent to which deep tremor  
25 signals are prevalent along plate boundaries elsewhere, including the Mediterranean basin, has  
26 not yet been documented in detail. A body of evidence suggests that tremor triggered during the  
27 surface waves of teleseismic events may commonly occur where ambient tremor during Episodic  
28 Tremor and Slip episodes occur, suggesting triggered tremor provides a useful tool to identify  
29 regions with ambient tremor. We perform a systematic search of triggered tremor at four major  
30 fault systems within the central-eastern Mediterranean basin, namely the Hellenic and Calabrian  
31 subduction zones, and the North Anatolian and Kefalonia transform faults, associated with large  
32 teleseismic events between 2010 and 2020. In addition, we search for ambient tremor during a  
33 ~50-daylong slow slip event in the eastern Sea of Marmara along a secondary branch of the  
34 North Anatolian Fault, and two ~4-month long slow slip events beneath western Peloponnese.  
35 We find no unambiguous evidence for deep triggered tremor nor for ambient tremor. The  
36 absence of triggered tremor at the Hellenic and Calabrian subduction zones supports the less  
37 favorable conditions for tremorgenesis in the presence of old and cold slabs. The absence of  
38 tremor along the transform faults may be due to an absence of the conditions commonly  
39 promoting tremorgenesis in such settings, including high fluid pressures and low differential  
40 stresses between the down-dip limit of the seismogenic layer and the Moho.

## 41 **1 Introduction**

42 The enhancement of geodetic and seismological monitoring systems over the last two  
43 decades has led to the discovery of various types of earthquakes, also known as slow  
44 earthquakes, with rupture velocities ranging from those of traditional earthquakes with rupture  
45 velocities ~2-3 km/s to roughly an order of magnitude faster than plate convergence rates, a few  
46 cm/yr (Obara, 2002; Rogers and Dragert, 2003; Obara and Kato, 2016). The range of speeds at  
47 which slip is accommodated is usually a function of depth, and may have implications for how  
48 plate tectonic loading stress is transferred along dip in major faults, therefore the analysis and  
49 interplay of slow and seismogenic earthquakes along fault zones is of particular interest  
50 (Schwartz and Rokosky, 2007; Obara and Kato, 2016). Slow earthquakes typically include  
51 seismically and geodetically observed events that vary over a range of characteristic time scales

52 (Obara and Kato, 2016). Seismically observed slow earthquakes include Low Frequency  
53 Earthquakes (LFEs) and non-volcanic tremor (hereafter referred to as tremor), with energy often  
54 concentrated between frequencies of 2-8 Hz (Obara, 2002), and Very Low Frequency  
55 Earthquakes (VLFs) with energy concentrated between 0.02-0.05 Hz (Ito et al., 2007).  
56 Geodetically observed slow earthquakes tend to exhibit slower rupture velocities that do not  
57 generate seismic energy, and are subdivided into short-term and long-term Slow Slip Events  
58 (SSEs) with durations of days to weeks and months to years, respectively (Wallace et al., 2012;  
59 Obara and Kato, 2016). The occurrence of tremor, mostly composed of bursts of LFEs (Shelly et  
60 al., 2007), is usually accompanied by short-term SSEs and VLFs (Obara and Kato, 2016). The  
61 coupled manifestation of tremor and short-term SSEs was first discovered in the Cascadia  
62 subduction zone (Rogers and Dragert, 2003) and has been termed Episodic Tremor and Slip  
63 (ETS). Tremor occurring during ETS episodes is also referred to as spontaneous or ambient  
64 tremor.

65         Several studies locate ETS episodes in subduction zones slightly deeper than the down-  
66 dip limit of the seismogenic zone, at depths spanning the intersection of the down-going slab and  
67 the upper-plate Moho (Obara, 2002; Wech and Creager, 2008; Brown et al., 2009; Ghosh et al.,  
68 2009b; Ide, 2012). ETS episodes along transform plate boundaries, where observed, mostly  
69 outline the upper boundary of continental Moho (Nadeau and Dolenc, 2005; Shelly, 2017).  
70 Although more widely studied, ETS episodes are not restricted to the down-dip portion of the  
71 seismogenic zone (Saffer and Wallace, 2015 and references therein). They have been also  
72 documented up-dip or within the seismogenic zone (e.g. Costa Rica, Walter et al., 2011, 2013;  
73 NE Japan trench, Nishikawa et al., 2019). In the following, we refer to ETS located below the  
74 down-dip limit of the seismogenic zone as deep ETS. The existing ~10-20 km gap between the  
75 deep ETS zone and the down-dip limit of the seismogenic layer is often filled by long-term SSEs  
76 (Obara, 2011; Husker et al., 2012; Wech, 2016; Gao and Wang, 2017) and does not appear to be  
77 strongly correlated to tremor and VLFs (Husker et al., 2012; Obara, 2011).

78         Although the underlining physical mechanisms remain enigmatic, it is commonly  
79 accepted that slow earthquakes may straddle a transitional physical state between conditions  
80 favoring stick-slip behavior and conditions favoring stable sliding (Audet and Kim, 2016). It also  
81 appears that fault thermal structure affects the depth distribution and occurrence of slow  
82 earthquakes (Ide, 2012; Yabe et al., 2014; Gao and Wang, 2017) due to the primary temperature

83 control on the brittle-plastic transition (Scholz, 1998). Numerical models with thermo-  
84 petrologically controlled rheology suggest the occurrence of the brittle-plastic transition at  
85 depths shallower than the upper-plate Moho as *conditio sine qua non* for slow earthquake  
86 occurrence in subduction zones (Gao and Wang, 2017). In fact, tremor has been primarily  
87 observed at young, warm subduction zones (Obara, 2002; Wech and Creager, 2008; Brown et al.,  
88 2009; Ide, 2012) where the brittle-plastic transition and peak dehydration reactions occur at  
89 shallower depths than in cold subduction zones (Peacock and Wang, 1999). However, the  
90 thermal structure of faults can be controlled by factors other than age (Yabe et al., 2014; Gao and  
91 Wang, 2017). For example, the often observed patchy nature of spatial deep tremor distribution  
92 (Ghosh et al., 2009b; Ide, 2012), indicates that tremor is also affected by other mechanisms such  
93 as pore fluid pressure (Kodaira et al., 2004; Audet et al., 2009), rock frictional properties  
94 (Houston, 2015), fault geometrical complexities (Romanet et al., 2018), sea floor irregularities  
95 and properties of overriding plate (Nishikawa et al., 2019). Seismological investigations often  
96 reveal the presence of near-lithostatic pore fluid pressures (e.g. high  $V_p/V_s$  ratios) in regions  
97 where tremor does occur (Kodaira et al., 2004; Audet et al., 2009; Audet and Kim, 2016;).  
98 Hence, the presence of high fluid pressure that reduces the effective stresses and the frictional  
99 strength along the fault is the mechanism most commonly invoked to control deep tremor  
100 generation within a transitional physical state (Kodaira et al., 2004; Audet and Kim, 2016; Gao  
101 and Wang, 2017). Similar conditions are proposed to control tremor generation up-dip of the  
102 seismogenic zone in subduction zones (Saffer and Wallace, 2015). Hence, potentially  
103 tremorgenic conditions could exist along many faults and possibly at different depths. However,  
104 to date, the description of favorable and non-tremorgenic conditions is practically limited to the  
105 observations along the Pacific rim and does not extend to fault systems where diverse physical  
106 and geological conditions may coexist such as in the Mediterranean basin.

107 In fault zones where ambient tremor is observed during ETS episodes, it is also  
108 commonly triggered during the passing of surface waves from teleseismic events (hereafter  
109 referred to as triggered tremor) (Fig. 1; e.g. Gomberg et al., 2008; Miyazawa et al., 2008;  
110 Miyazawa and Brodsky, 2008; Peng and Chao, 2008; Ghosh et al., 2009a; Fry et al., 2011; Chao  
111 et al., 2012a, 2012b, 2013). As triggered tremor typically has larger amplitudes than ambient  
112 tremor (Rubinstein et al., 2007), a systematic search for triggered tremor provides a useful tool to  
113 identify regions that might also experience (undocumented) ambient tremor.

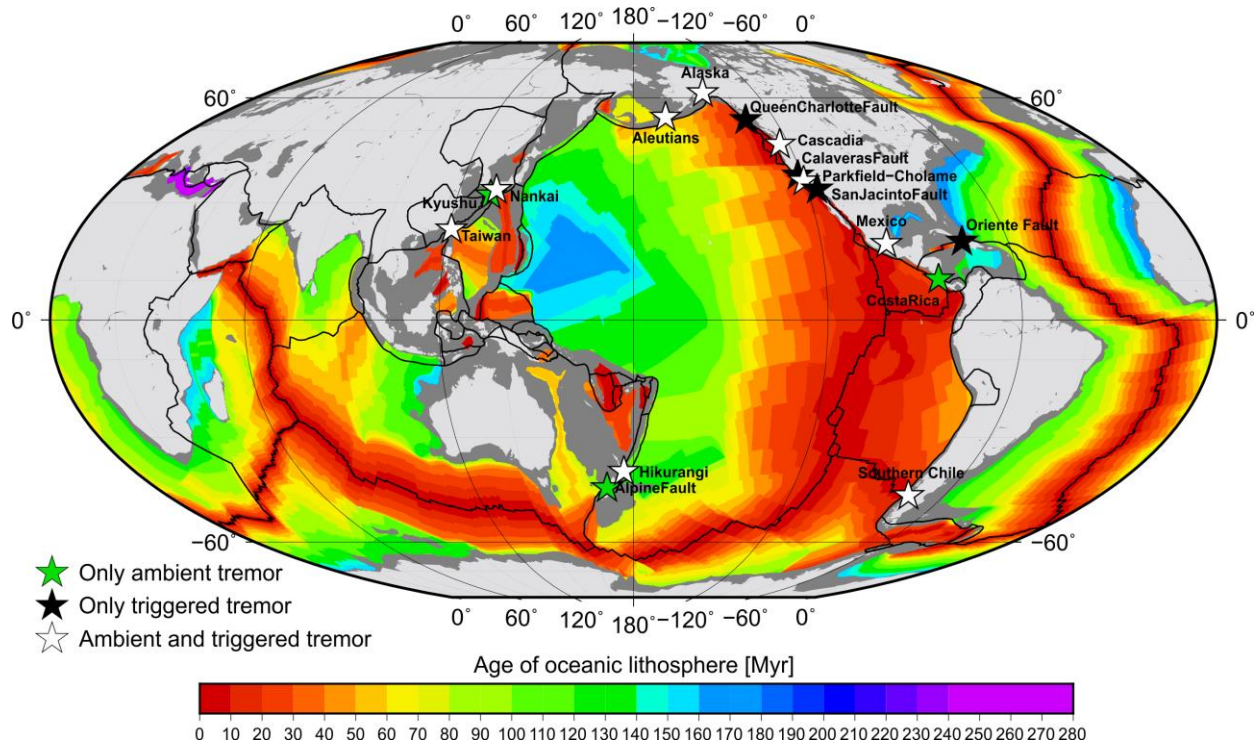


**Figure 1.** Global distribution of well-documented (observed at a minimum of three stations) sources of triggered and ambient tremor, which is confined primarily to the Pacific rim (Nadeau and Dolenc, 2005; Brown et al., 2009, 2013; Peng et al., 2009; Kim et al., 2011; Chao et al., 2012a, 2013; Ide, 2012; Wech et al., 2012; Aiken et al., 2013; Sun et al., 2015; Nishikawa et al., 2019). Note the inverse correlation between the occurrence of tremor and the age of the subducting oceanic lithosphere, which is colored according to age (Müller et al., 2008).

115        Teleseismically induced Peak Ground Velocities (PGV) as low as 0.01-0.03 cm/s,  
 116 corresponding to dynamic stresses of about 1-3 kPa, are also capable of triggering tremor  
 117 (Miyazawa and Brodsky, 2008; Peng et al., 2009; Chao et al., 2012a). Tremor triggering  
 118 thresholds appear to be variable from region to region (Peng and Gomberg, 2010) and may  
 119 depend on several factors including instrumentation differences and background tremor activity  
 120 (Chao et al., 2012a). Furthermore, in some locations, tidally induced stress changes on the order  
 121 of ~1 kPa seem to be capable of triggering tremor (Thomas et al., 2009; Houston, 2015; van der  
 122 Elst et al, 2017). Despite the growing observations of ambient and triggered tremor, one of the  
 123 most striking features of all well-documented cases (i.e. visible at least at three seismic stations),  
 124 is that they are confined to transform and convergent plate boundaries, or fault systems, along  
 125 the Pacific rim (Fig. 1). To date, the Oriente Fault near Guantanamo Bay (Cuba) represents the  
 126 only exception with observed triggered tremor during two teleseismic events (Peng et al., 2013).  
 127 Whether the absence (or infrequent occurrence) of deep tremor outside of the Pacific rim is due

128 to a sampling bias or to non-favorable physical conditions is still poorly understood. The dearth  
129 of studies reporting null results, i.e. an absence of tectonic tremor (Yang and Peng, 2013;  
130 Bockholt et al., 2014; Pfohl et al., 2015) make it hard to address such a question.

131 In this work, we perform a systematic search of triggered tremor within the central-eastern  
132 Mediterranean basin (Fig. 2). The region is generally well instrumented due to its intense seismic  
133 activity, and therein subduction zones exhibit different physical (e.g. old/cold subducting  
134 lithosphere and slower converge rates) and depositional conditions (e.g. thicker and wider  
135 accretionary wedges) compared to the Pacific rim. Moreover, for instance, its major transform  
136 faults, namely the Kefalonia and North Anatolian Fault, have formed more recently and have  
137 accumulated smaller relative displacement (Şengör et al., 2005; van Hinsbergen et al., 2006) than  
138 the Alpine and San Andreas Faults (Dickinson and Wernicke, 1997; Norris and Cooper, 2001),  
139 where tremor has been documented (Fig. 1). Hence, it is well suited to further explore necessary  
140 and inhibiting physical conditions for tremor occurrence. In the specific, we focus on four major  
141 active fault systems, namely the Hellenic and Calabrian subduction zones, and the Kefalonia and  
142 Marmara section of the North Anatolian transform faults (Fig. 2), where no unambiguous  
143 example of ambient and triggered tremor has been reported to date. In all analyzed regions,  
144 sufficient seismic station coverage was available over the past 10 years which is sufficient to  
145 detect triggered tremor, should it have occurred. Although the main focus of this study is  
146 triggered tremor, we also investigate the occurrence of ambient tremor during a SSE in the  
147 eastern Marmara Sea, along the North Anatolian Fault, and two SSEs beneath Peloponnese, in  
148 the western segment of the Hellenic Subduction Zone.

149 We limit our analysis to subduction zones and transform faults because they host the  
150 multitude of observed triggered and ambient deep tremor worldwide (Fig. 1). In Section 2 we  
151 provide a tectonic overview of the study regions, followed by a description of the datasets and  
152 methods in Section 3. We report the results in Section 4 and discuss, together with the  
153 implications of our study, the similarities and differences with other fault systems in Section 5.  
154 Conclusive remarks of the study are in Section 6.

## 155 **2 Plate Boundaries in the central-eastern Mediterranean**

156 The current tectonic setting of the Mediterranean area arose from a complex interaction  
157 between the long-lasting but comparatively slow convergence of the African and Eurasian plates

158 (Faccenna et al., 2014). Deformation concentrates along irregular and diffuse boundaries  
159 between fragments of continental and oceanic lithosphere moving independently from the overall  
160 convergent motion (Fig. 2) (Faccenna et al., 2014). Historical and instrumental seismicity,  
161 defined by frequent low-to-moderate and occasionally large ( $M > 7$ ) magnitude earthquakes  
162 (Guidoboni and Comastri, 2005), concentrates along the plate and microplate boundaries (Fig.  
163 2). Compared to the western portion, the central-eastern Mediterranean basin releases larger  
164 seismic moment and displays larger strain rates (Martínez-Garzón et al., 2020). The oldest *in situ*  
165 oceanic lithosphere on Earth ( $>220$ - $230$  Ma) is currently subducting at the Hellenic and  
166 Calabrian Arcs (Granot, 2016; Müller et al., 2008; Speranza et al., 2012). These very narrow and  
167 arcuate subduction arcs (Faccenna et al., 2014), and the thick and wide accretionary prisms (Clift  
168 and Vannucchi, 2004) make the Mediterranean basin a unique region worldwide (Fig. 1-2).

169 In this region, the occurrence of slow earthquakes is still poorly investigated, and, to date,  
170 there is no unambiguous evidence of deep tectonic tremor in the Mediterranean basin. The  
171 Hellenic (Fig. 2c) and Calabrian (Fig. 2b) subduction zones, as well as the Kefalonia (Fig. 2a)  
172 and North Anatolian transform faults (Fig. 2d), share similar faulting styles with those of fault  
173 systems where deep tremor has been documented and therefore represent potential candidates for  
174 hosting deep tremor in the central-eastern Mediterranean.

175 Although all formed in the broad tectonic context of Africa-Eurasia convergence, the four  
176 fault systems developed at different times and present distinct seismotectonic settings (e.g.  
177 kinematics, seismic moment release, age). In the following subsections (2.1-2.4) we delineate the  
178 main seismotectonic properties of the regions selected for the search for tremor. We focus on the  
179 description of seismotectonic and geological aspects that are relevant to deep tremorigenic  
180 conditions.

## 181 2.1 The Kefalonia Transform Fault

182 The Kefalonia Transform Fault (Fig. 2a) marks the western termination of the Hellenic  
183 Subduction Zone (Louvari et al., 1999; Pérouse et al., 2012; Bocchini et al., 2018). It started to  
184 form in the late Miocene-early Pliocene and has accumulated most of its  $\sim 60$  km of total  
185 displacement over the last  $\sim 4$ - $5$  Ma (van Hinsbergen et al., 2006). The fault accommodates  $\sim 2$   
186 cm/yr of differential convergence between oceanic subduction and continental collision taking  
187 place to the north and south, respectively (Pérouse et al., 2012). It is composed primarily of two

188 active segments, namely the Kefalonia and the Lefkada segments (Fig. 2a) and exhibits pure  
189 right-lateral or transpressional slip motion (Louvari et al., 1999). The fault frequently generates  
190  $M > 6$  earthquakes (Papazachos and Papazachou, 2003; Papadimitriou et al., 2017). The  
191 distribution of earthquakes suggests a seismogenic layer extending between 3 and 16 km  
192 (Papadimitriou et al., 2017), with a crustal Moho at  $\sim 28$  km (Sodoudi et al., 2006). To date there  
193 is no documented evidence of slow earthquakes along the Kefalonia Transform Fault.

## 194 2.2 The Calabrian Subduction Zone

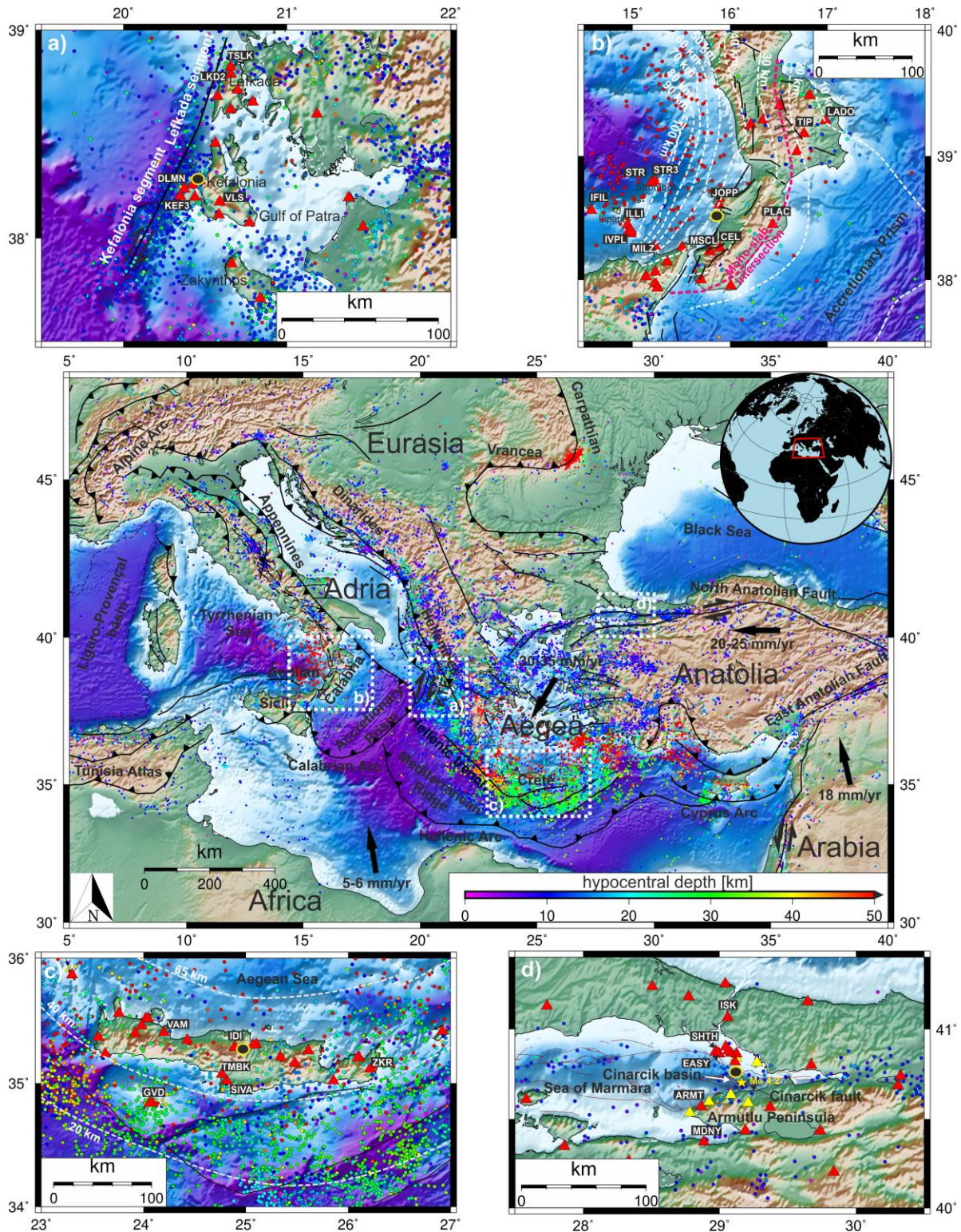
195 The Calabrian Subduction Zone (Fig. 2b) forms a narrow, arcuate subduction interface in  
196 southern Italy. The subduction of  $\sim 220$ - $230$  Ma old oceanic crust (Speranza et al., 2012) began  
197  $\sim 80$  Ma ago (Faccenna et al., 2001), and currently continues along a  $\sim 150$  km wide sector  
198 between the Isthmus of Catanzaro to the north and the Strait of Messina to the south (Fig. 2b)  
199 (Maesano et al., 2017). The incoming plate has a 5-6 km thick layer of sedimentary cover  
200 forming a large accretionary prism (de Voogd et al., 1992). The subduction convergence rate is  $<$   
201  $5$  mm/yr (Pérouse et al., 2012), and has documented intraslab seismicity down to  $\sim 450$ - $500$  km  
202 (Selvaggi and Chiarabba, 1995), as well as a depletion of shallow interplate seismicity offshore  
203 in the Ionian Sea. The very low interplate seismicity and the low strain rates in the forearc ( $\sim 10$ -  
204  $20$  nanostrain/yr) led some authors to consider the subduction as inactive (e.g. Pérouse et al.,  
205 2012). However, a recent study interprets unambiguous geodetic signals consistent with elastic  
206 strain accumulation at the megathrust being released episodically seismically and/or more likely  
207 through aseismic slip transients (Carafa et al., 2018). The interpretation also reconciles with the  
208 large historical earthquake data in Calabria (Carafa et al., 2018), and could suggest the  
209 occurrence of slow earthquakes.

## 210 2.3 The Hellenic Subduction Zone

211 The Hellenic Subduction Zone (Fig. 2) defines an approximately 1000 km long arcuate  
212 interface bounded to west by the Kefalonia Transform Fault and to the east, beneath south-  
213 western Turkey, by a tear in the slab (Bocchini et al., 2018). Oceanic lithosphere of age  $>220$ -  
214  $230$  Ma to the west (Speranza et al., 2012), and likely  $>300$  Ma to the east (Granot, 2016) is  
215 currently subducting at a rate of  $\sim 35$ - $40$  mm/yr (McClusky et al., 2000). The down-going plate is  
216 overlaid by a wide sediment layer forming the Mediterranean Ridge Accretionary Prism which

217 spans roughly up to 10-12 km thickness and is ~250-300 km long (e.g. Bohnhoff et al., 2001;  
218 Kopf et al., 2003). Nubian-Aegea convergence generates intense seismicity, even for  $M > 4$  (Fig.  
219 2), and earthquakes as large as  $M \sim 8$  as reported in historical catalogues (Papazachos and  
220 Papazachou, 2003). Seismological and geodetic studies suggest that more than 70-80% of the  
221 relative plate motion occurs aseasonally (Becker and Meier, 2010; Vernant et al., 2014;  
222 Saltogianni et al., 2020). Very recently, Mouslopoulou et al. (2020) reported two SSEs beneath  
223 the western coast of Peloponnese south of Zakynthos (Fig. 1Sb). Both SSEs were preceded by ~2  
224 months of plate motion acceleration. The first geodetic transient started on 09/24/2014 and  
225 terminated on 03/20/2015, with the actual SSE starting on 11/29/2014. The second started on  
226 05/14/2018 and terminated on 10/25/2018, with the actual SSE starting on 07/10/2018. Both  
227 SSEs are suggested to occur between 20 and 40 km depth along the plate interface. To date, no  
228 evidence of tectonic tremor is reported along the active margin between the down-going and  
229 overriding plates.

230 Crete represents a horst structure in the central Hellenic forearc (Fig 2c) currently  
231 undergoing fast uplift and extension (Meier et al., 2007). Subduction south of Crete started about  
232 20–15 Ma, when the plate boundary stepped back to the southern edge of an accreted  
233 microcontinent, building most of the continental crust of present Crete (Thomson et al. 1998).  
234 The megathrust south of Crete, exhibits intense microseismicity that abruptly terminates at ~40  
235 km depth below the southern coastline of the island (Meier et al., 2004), where the upper-plate  
236 crustal thickness is ~30-35 km (Bohnhoff et al., 2001; Meier et al., 2007).



237

**Figure 2.** Main panel: Central and eastern Mediterranean region. Main tectonic elements (black lines) from Faccenna et al., (2014). Black arrows indicate the relative plate-microplate motion with respect to stable Eurasia (McClusky et al., 2000). Earthquake hypocentral locations (dots) are color coded according to depth, saturated to 50 km. We plot all earthquakes with  $M > 4$

documented by the International Seismological Centre (ISC) between 1964-2010 (ISC, 2020). Dotted white boxes in the main panel indicate the four study regions: a) Kefalonia Transform Fault, b) Calabrian Subduction Zone; c) Hellenic Subduction Zone, Crete; d) North Anatolian Fault, eastern Marmara Sea. Red triangles indicate the maximum number of available seismic stations (not necessarily available in all investigated periods), where station names used in Fig. 4 are shown in white. Yellow triangles in panel c indicate borehole stations. Dashed lines in panels b-c represent the top of the slab isodepths from Maesano et al., (2017) and Bocchini et al., (2018), respectively. Dashed magenta line in panel b indicates the location of the intersection with the overriding plate Moho. Yellow star in panel (d) indicates the epicentral location of the Mw 4.2 Yalova earthquake on June 25, 2016. Black circles with yellow edges indicate the location where initial Peak Ground Velocity values were estimated (see Section 3). Bathymetry is from Ryan et al., (2009).

#### 238 2.4 The North Anatolian Fault.

239 The North Anatolian Fault is a 1200-km-long right-lateral transform fault forming the  
 240 boundary between the Eurasian Plate and the Anatolian microplate with relative displacement of  
 241 ~20-25 mm/yr (Fig. 2) (McClusky et al., 2000). It started to form 12-13 Ma ago during the late  
 242 phase of Arabia-Eurasia collision that accumulated a maximum displacement of ~85-90 km  
 243 decreasing from east to west (Bohnhoff et al., 2016). The North Anatolian Fault is well-known  
 244 for its intense seismicity and frequent  $M > 7$  earthquakes (Bohnhoff et al., 2016), such as the  
 245 earthquake sequence in the 20th century that ruptured all but the Sea of Marmara segments  
 246 (Stein et al., 1997). The Sea of Marmara region (Fig. 2d) representing the western portion of the  
 247 North Anatolian Fault is in a transtensional state and represents a pull-apart basin within two  
 248 major branches of the North Anatolian Fault that are ~100 km apart (Armijo et al., 2002). It  
 249 formed as part of a NS-extensional regime related to the fast rollback of the Hellenic Subduction  
 250 Zone with the strike-slip regime being active since ~2.5 Ma (Şengör et al., 2005; Le Pichón et  
 251 al., 2016). The northern part of the Sea of Marmara is characterized by the presence of three deep  
 252 basins separated by bathymetric highs, from east to west: the Çınarcık, Central, and Tekirdag  
 253 basins (Armijo et al., 2002). The Çınarcık basin is bounded to the south by the Çınarcık fault and  
 254 formed ~1.7-2.0 Ma accommodating ~2 km of N-S extension and ~18 km of right-lateral  
 255 deformation (Carton et al., 2007). Precise hypocentral solutions suggest a seismogenic layer  
 256 extending down to 10-15 km in the eastern Sea of Marmara (Wollin et al., 2018) while the Moho  
 257 is found at 26-41 km depth (Zor et al., 2006; Jenkins et al., 2020).

258 The analysis of recent high temporal resolution geodetic data revealed the existence of  
 259 temporal fluctuations of the creep rate with detection of accelerating bursts of shallow (i.e. 0-5

260 km) creep events (i.e. SSEs) along the segments of the North Anatolian Fault that ruptured  
261 during the 1999 Izmit earthquake (Aslan et al., 2019) and the 1944 Ismetpasa earthquake  
262 (Rousset et al., 2016). On 25 June 2016, a ~50-daylong SSE was recorded along the Çınarcık  
263 fault below the eastern Sea of Marmara (Martínez-Garzón et al., 2019). The authors obtain the  
264 best fit between calculated and observed signal, assuming the source location to be near to the  
265  $M_w$  4.2 Yalova earthquake (Malin et al., 2018) occurred during the onset of the SSE (Fig. 2d).  
266 The strain release during the SSE was equivalent to a  $M_w$  5.8 at the depth of 9 km (Martínez-  
267 Garzón et al., 2019). However, the depth remains poorly constrained due to its recording at a  
268 single station.

269 A previous study found no evidence for triggered tremor and no unambiguous evidence  
270 for ambient tremor on the central segment of the North Anatolian Fault near Ismetpasa (Pfohl et  
271 al., 2015), while here we focus on the recently densely instrumented eastern Sea of Marmara  
272 (Fig. 2d).

### 273 **3 Data and Methods**

274 In the description that follows, we restrict the analysis in the Hellenic Subduction Zone to  
275 the segment south of Crete due to the higher open-access seismic station density and data quality  
276 relative to adjacent segments. For the North Anatolian Fault, we focus on the eastern Sea of  
277 Marmara because of the waveform data from dense local network deployments that are available.  
278 In addition, we search for ambient tremor in the eastern Sea of Marmara, eventually related to  
279 the ~50-daylong SSE and the  $M_w$  4.2 event along the Çınarcık fault (Fig. 2d) on June 25, 2016  
280 (Martínez-Garzón et al., 2019), and during the two ~6-month long aseismic transients, and  
281 related SSEs, beneath Peloponnese, along the western segment of the Hellenic Subduction Zone  
282 (Mouslopoulou et al., 2020).

283 As a first criteria to search for triggered deep tremor, we identify prospective triggering  
284 teleseismic earthquakes by selecting all events with  $M_w \geq 6.5$ , hypocentral depths  $\leq 50$  km, and  
285 epicentral distances  $\geq 800$  km that generated a theoretical PGV larger than 0.01 cm/s within each  
286 study region. We restrict our analysis to large and shallow potential triggering mainshocks  
287 because they are most effective in generating large surface waves at teleseismic distances, and  
288 hence have the greatest potential of triggering tremor. We calculate theoretical PGV values at a

289 point in the middle of each study region (Fig. 2a-d) using a ground motion empirical relationship  
290 (Aki and Richards, 2002; Lay and Wallace, 1995):

$$291 \quad M_s = \log A_{20} + 1.66 \log \Delta + 2.0 \quad (1)$$

$$292 \quad PGV \approx 2\pi A_{20}/T \quad (2)$$

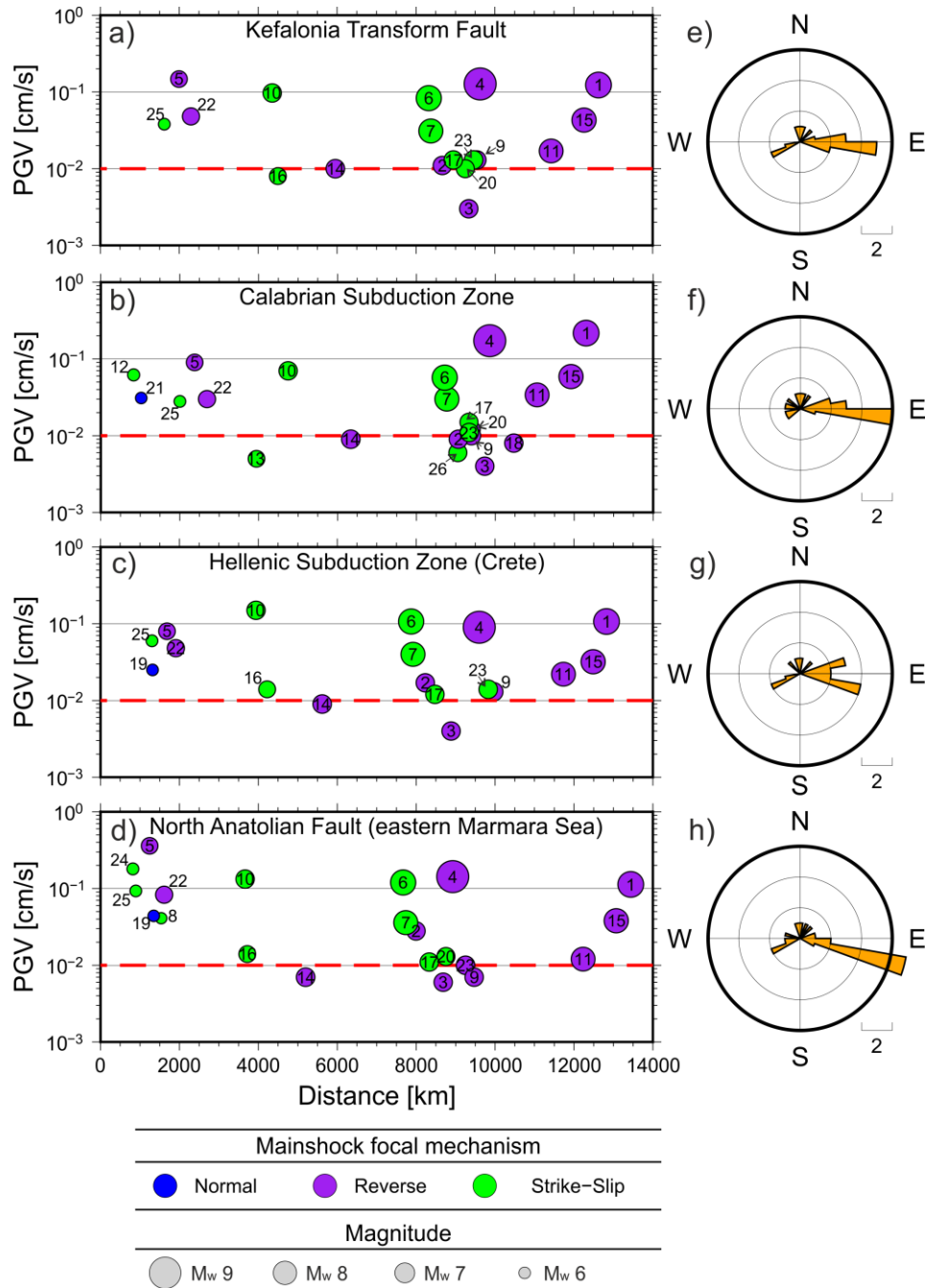
293 where  $M_s$  is the surface wave magnitude,  $A_{20}$  is the amplitude (in microns) of the Airy  
294 phase (surface wave with a 20 s period),  $\Delta$  is the source-receiver (epicentral) distance, and  $T$  is  
295 the surface wave period (20 s). We assume  $M_s=M_w$  as first approximation. We download all  
296 mainshock candidate waveforms from the European Integrated Data Archive (EIDA,  
297 <http://www.orfeus-eu.org/data/eida/>). In addition to publicly available data, we use data from  
298 dense local deployments, namely the PIREs network (GFZ Potsdam BU-Kandilli, 2006) and the  
299 GONAF borehole network (Bohnhoff et al., 2017) to search for triggered tremor in the eastern  
300 Sea of Marmara.

301 As a second criteria for culling the list of candidate mainshocks, we calculate the  
302 observed  $PGV_{obs}$  value as the average value between the three components from all the available  
303 broad-band stations within each region (Fig. 2a-d), and reject the events which average  $PGV_{obs} <$   
304  $0.01$  cm/s (Fig. 3a-d). We retain a total of 16 candidates for the Hellenic and Calabrian  
305 subduction zones and for the Kefalonia Transform Fault and 18 events for the North Anatolian  
306 Fault (Fig. 3 a-d, Table S1). A complete list of analyzed events is reported in Table S1. Nearly all  
307 selected mainshocks are either strike-slip or reverse faulting earthquakes (Fig. 3a-d). They cover  
308 a wide range of back azimuthal directions, with a limited gap to the south (Fig. 3e-h).

309 To manually search for cases of triggered tremor, we visually inspect waveforms  
310 surrounding the time interval predicted for the passage of surface waves in each study region.  
311 We calculate theoretical surface wave arrivals using the TauP package and the iasp91 velocity  
312 model (Kennett and Engdahl, 1991) in Obspy (<https://docs.obspy.org/packages/obspy.taup.html>),  
313 and search temporal windows starting when a phase travelling at 4.4 km/s (approximate Love  
314 wave arrival) reaches the station and terminates with the predicted arrival of a Rayleigh phase  
315 travelling at 2.0 km/s. The time window choice ensures that Love and Rayleigh waves with the  
316 highest triggering potential and amplitudes are included in the analysis. We rotate horizontal  
317 components to transverse and radial directions to visually confirm the correct arrival time of  
318 Love and Rayleigh waves, respectively. Following a well-established procedure, we search for

319 non-impulsive, coherent signals, applying either a 2-8 Hz bandpass filter or a 5 Hz highpass filter  
320 to remove the low-frequency teleseismic signal (i.e. primary and secondary arrivals) and  
321 preserve tremor signals in the frequency band where it is commonly observed to be most  
322 energetic. We require any prospective triggered tremor signal to be recorded by at least three  
323 seismic stations in order to be sure that the signal is local and of tectonic origin.

324 In addition to visual inspection, we also employ an envelope cross-correlation (Ide, 2012,  
325 2010) to detect ambient tremor during the SSE in the eastern Sea of Marmara during an extended  
326 time period from (06/02/2016 to 07/30/2016) encompassing the SSE (Martínez-Garzón et al.,  
327 2019) and the two SSEs, in 2014-2015 and in 2018, along the western segment of the Hellenic  
328 Subduction Zone (Mouslopoulou et al., 2020). The procedure entails creating daily envelopes of  
329 signals filtered between 2 and 8 Hz and cross-correlating horizontal channels at stations located  
330 <100 km apart. An event is detected when a minimum cross-correlation value (0.5-0.7) is  
331 exceeded at a minimum number of channels (5-8). A more detailed description of the method is  
332 available at Ide (2010; 2012) and it is also provided in the supplement along with details on the  
333 station configuration (Text 1S). In Figure 2S, we report an example of ambient tremor detected  
334 using the envelope cross-correlation method employed in this study (Fig. 2S). We detect several  
335 tremor signals near the Parkfield-Cholame segment of the San Andreas Fault, where tremor is  
336 widely documented (Nadeau and Dolenc, 2005; Shelly, 2017), using the same settings as for the  
337 eastern Sea of Marmara (Fig. 2S). We are aware of the limitations of the detection method in the  
338 absence of the dense network coverage (Fig. 1S) that is needed to detect low amplitude  
339 correlated signals, particularly in the presence of intense background seismic activity that could  
340 mask possible tremor signals. However, although search of triggered tremor remains the focus of  
341 the paper, the occurrence of SSEs that could be associated with the occurrence of LFE/tremor  
342 activity warrants an additional search for ambient tremor.



343

**Figure 3.** List of candidate mainshocks around which the search for triggered deep tremor is centered (a-d). (a-d) Symbol sizes correspond to magnitude, while color code corresponds to focal mechanism type. Dotted red lines indicate lower threshold of 0.01 cm/s Peak Ground Velocities (PGV) considered for mainshock candidates in this study. Observed PGV ( $PGV_{obs}$ ) is calculated as the average value (unfiltered traces) among the three components of all the available broad-band stations within each region. (e-h) Back azimuths of candidate mainshocks producing  $PGV_{obs} > 0.01$  cm/s. Numbers are event IDs and associated events are reported in Table S1.

## 344 **4 Results**

345 The manual inspection of waveforms during the passage of surface waves from events in  
346 Table S1 at seismic stations along four major fault systems within the central-eastern  
347 Mediterranean basin reveals no unambiguous case of triggered tremor at any of the study areas,  
348 nor for ambient tremor during the documented SSEs. We first document the observations for  
349 triggered tremor (4.1), followed by ambient tremor below (4.2).

### 350 4.1 Triggered tremor

351 We find no unambiguous evidence for triggered tremor beneath Crete, along the Hellenic  
352 subduction zone, beneath Calabria at the Calabrian subduction zone, at the Kefalonia Transform  
353 Fault, and in the eastern Sea of Marmara, along the North Anatolian Fault, during the time period  
354 from 2010 to 2020 considered here. Although the minimum number of three stations may be a  
355 strict criterion relative to previous studies, we also do not observe coherent tremor-like signals if  
356 reducing the minimum number of required stations to two. In Figure 4, we show high frequency  
357 waveforms at a sample of stations during surface wave ground shaking of mainshock candidates  
358 inducing some of the largest  $PGV_{obs}$  within each region as a representative example of the lack  
359 of tremor energy.

360 We do observe potentially triggered low frequency signals at stations located along the  
361 Aeolian Arc, the volcanic arc of the Calabrian Subduction Zone (Fig. 2b). Two of the most  
362 striking signals are observed at station ILLI on Lipari Island (Fig. 3S) and at stations ISTR and  
363 IST3 on Stromboli (Fig. 4S). However, despite the good correlation between  $PGV_{obs}$  and low  
364 frequency signal occurrence, we cannot consider them as triggered signals. First, neither case  
365 fulfills the criterion of tremor-like signals exhibiting signal coherency at minimum three stations.  
366 In addition, careful inspection of the waveforms from one day before to one day after the  
367 mainshock reveals that the signal detected at station ILLI (Fig. 3S) is likely noise, due to the  
368 highly regular and repetitive nature of the candidate tremor signal (starting at ~6 am and ending  
369 at ~5 pm) in the frequency band of interest (2-8 Hz and higher). The signal we observe at  
370 stations ISTR and IST3 on Stromboli (Fig. 4S) is very likely a LFE of volcanic origin, however,  
371 we note that we also observe several LFEs events both before and after the ground shaking  
372 induced by the teleseismic event. Moreover, the slab interface at the closest stations to where the  
373 tremor-like signal is observed is located at ~100 km depth beneath the volcanic Arc (Maesano et

374 al., 2017). A seismic signal originating at 100 km depth would not support a seismic source  
375 originating from the ETS zone, which is expected at shallower depths where the slab intersects  
376 the overriding plate, corresponding to ~25 km depth at the observed location (Fig. 2b).

377 The seismic stations on Crete exhibit evidence for a single tectonic tremor candidate  
378 during the  $M_w$  8.3 Illapel (Chile) earthquake (ID 15 in Fig. 3, Tab. 1S). However, although  
379 visible at 3-4 stations (Fig. 5S) the signal is observed before the arrival of surface waves, when  
380  $PGV_{obs}$  is smaller than 0.01 cm/s, suggesting an ambient, rather than triggered origin. We  
381 explore the possibility that the detected signal (Fig. 5S) could represent ambient tremor by  
382 running match filter detection in EQcorrscan (Chamberlain et al., 2018). We used 6-8s second-  
383 long signal time windows, filtered between 2-8 Hz, to correlate with continuous data in one-day  
384 time windows before and after the tremor-like signal occurrence. Observations of ambient tremor  
385 in other fault zones rarely document isolated tremor events, but more commonly clustered,  
386 prolonged activity. The matched filter detection yielded no additional detections of similar low  
387 frequency signals, in spite of testing a range of settings.

388 At seismic stations along the Kefalonia Transform Fault we do not observe any tremor  
389 like signal. We observe, as in the other regions, possible dynamically triggered local earthquakes  
390 (see example in Fig. 4a), however, we will dedicate further investigation of remote dynamic  
391 earthquake triggering to a follow-up study, as the purpose of this work is to investigate the  
392 occurrence of tectonic tremor. Unfortunately, for the Kefalonia Transform Fault we have only 2-  
393 3 stations available during the passage of surface waves of the  $M_w$  8.8 2010 Maule and the  $M_w$   
394 9.1 2011 Tohoku earthquakes, the largest events occurred between 2010 and 2020.

395 Finally, we do not observe tremor activity during the passage of surface waves in the  
396 eastern Sea of Marmara. The latter represents the better instrumented region in our study.  
397 Observed correlated signals are either associated to local earthquakes or to instrument/cultural  
398 noise.

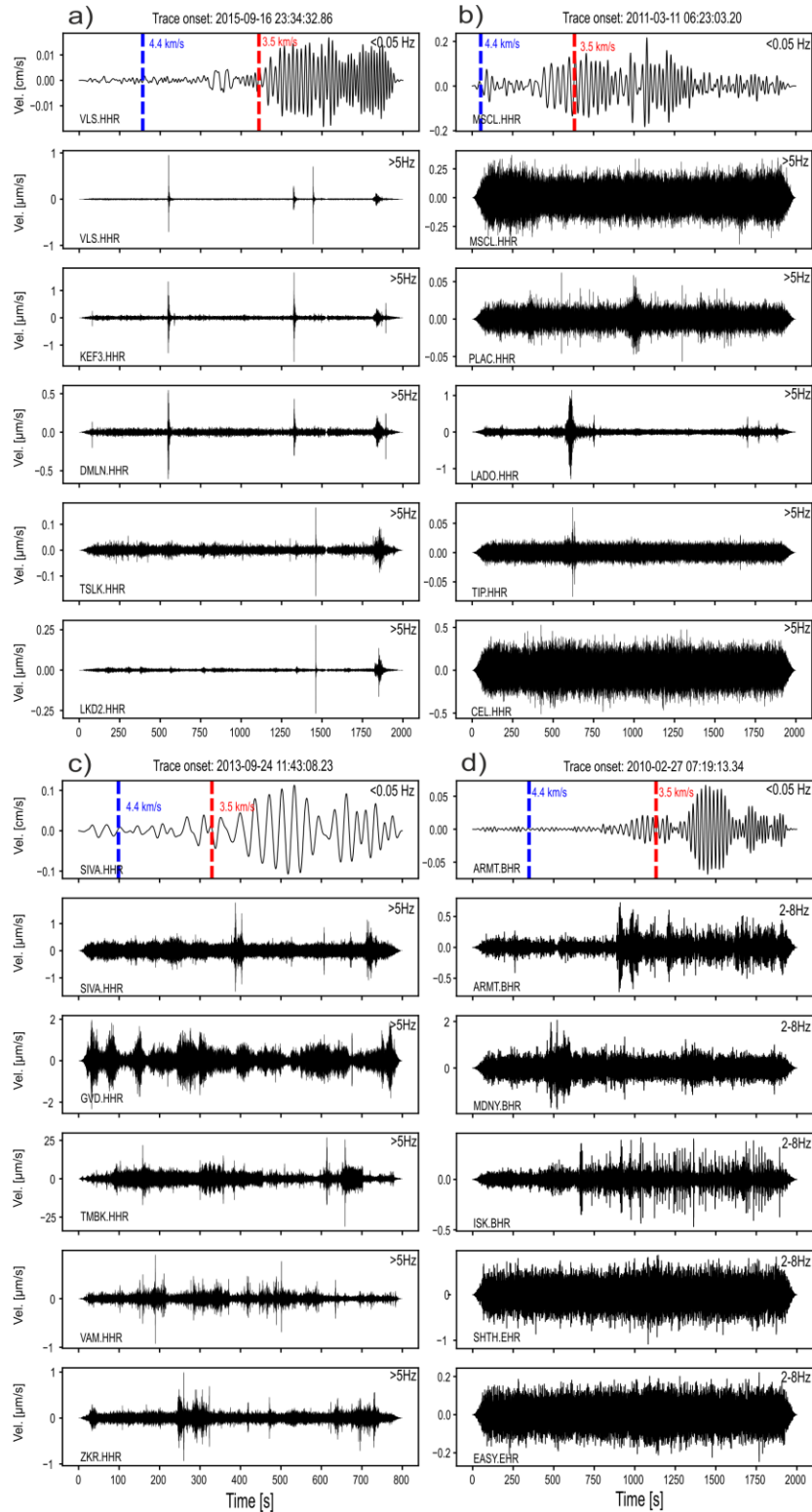


**Figure 4.** Example of waveforms exhibiting a lack of evidence for triggered tremor at the a) Kefalonia Transform Fault, during the  $M_w$  8.3 Illapel (Chile) earthquake (ID 15 in Fig.3 and Tab. 1S); b) Calabrian Subduction Zone, during the  $M_w$  9.1 Tohoku (Japan) earthquake (ID 3 in Fig.3 and Tab. 1S); c) Hellenic Subduction Zone (Crete), during the  $M_w$  7.8 Pakistan earthquake

(ID 10 in Fig.3 and Tab. 1S); d) Eastern Marmara Sea (North Anatolian Fault), during the  $M_w$  8.8 Maule (Chile) earthquake (ID 1 in Fig.3 and Tab. 1S). The candidate triggering earthquakes are among those generating the largest recorded  $PGV_{obs}$  locally (Fig. 3). The onset time of the signals in each region is indicated on top of each panel. Three clear local earthquakes (one between 500 and 750 sec and two between 1250 and 1500 sec) are visible at the Kefalonia Transform Fault (a), and a more distant earthquake is visible between 1750 and 2000 sec. In other regions, only uncorrelated noise is visible except for stations LADO and TIP at the Calabrian Subduction Zone (b) where a local signal is visible between 500 and 750 sec. The dashed red and blue lines in the topmost panels indicate the estimated arrival time of phases travelling at 4.4 and 3.5 km/s, respectively, used as preliminary arrival time of Love and Rayleigh waves. The location of seismic stations used herein is shown in Fig. 2a-d.

#### 399 4.2 Ambient tremor

400 We find no unambiguous examples of LFE/tremor activity accompanying the SSEs in the  
 401 eastern Marmara Sea and beneath western Peloponnese. Such result, although possibly affected  
 402 by the limitations described before in Section 3, are consistent with the absence of triggered  
 403 tremor along the investigated plate margins. As suggested by examples elsewhere in the world,  
 404 triggered tremor tends to occur in regions where also ambient tremor occurs (Fig. 1).

405 In addition to local earthquakes with energetic signals in the frequency band both higher  
 406 than 10 Hz and in the 2-8 Hz frequency band, we detect signals with dominant frequencies in the  
 407 tectonic tremor frequency band (2-8 Hz, Fig. 5). However, other factors suggest that the signals  
 408 as shown in Figure 5, are not tectonic tremor. The signal in Figure 5a has, at the closest station, a  
 409 duration  $> 15$  sec and a frequency content  $< 10$  Hz. However, at stations exhibiting a higher  
 410 Signal-to-Noise-Ratio (e.g. DRO Fig. 5a), the same signal more closely resembles a local  
 411 earthquake rather than tremor. We also detect signals (S-waves) from more distant earthquakes  
 412 that could be misinterpreted as an LFE if one restricted observation of such phases to stations  
 413 located near SSEs sources where tremor activity would be expected (Fig 5b). For example, the  
 414 signal shown in Figure 5b, exhibits low frequency energy at stations on the Armutlu Peninsula  
 415 (e.g. ARMT, KURT, YLV), however, at stations located to the west of the Marmara Sea (e.g.  
 416 KRBG, RKY) the typical character of an earthquake appears clear. Because of the occurrence of  
 417 several examples as those reported in Figure 5, we visually check all the detections. At the  
 418 Hellenic Subduction Zone, due to the longer cumulative duration of the two geodetic transients  
 419 ( $\sim 1$  year), we checked all detected signals with duration longer than 15 seconds (through a  
 420 preliminary investigation we observed that signals shorter than 15 seconds were mostly local  
 421 earthquakes and in very few cases noise).

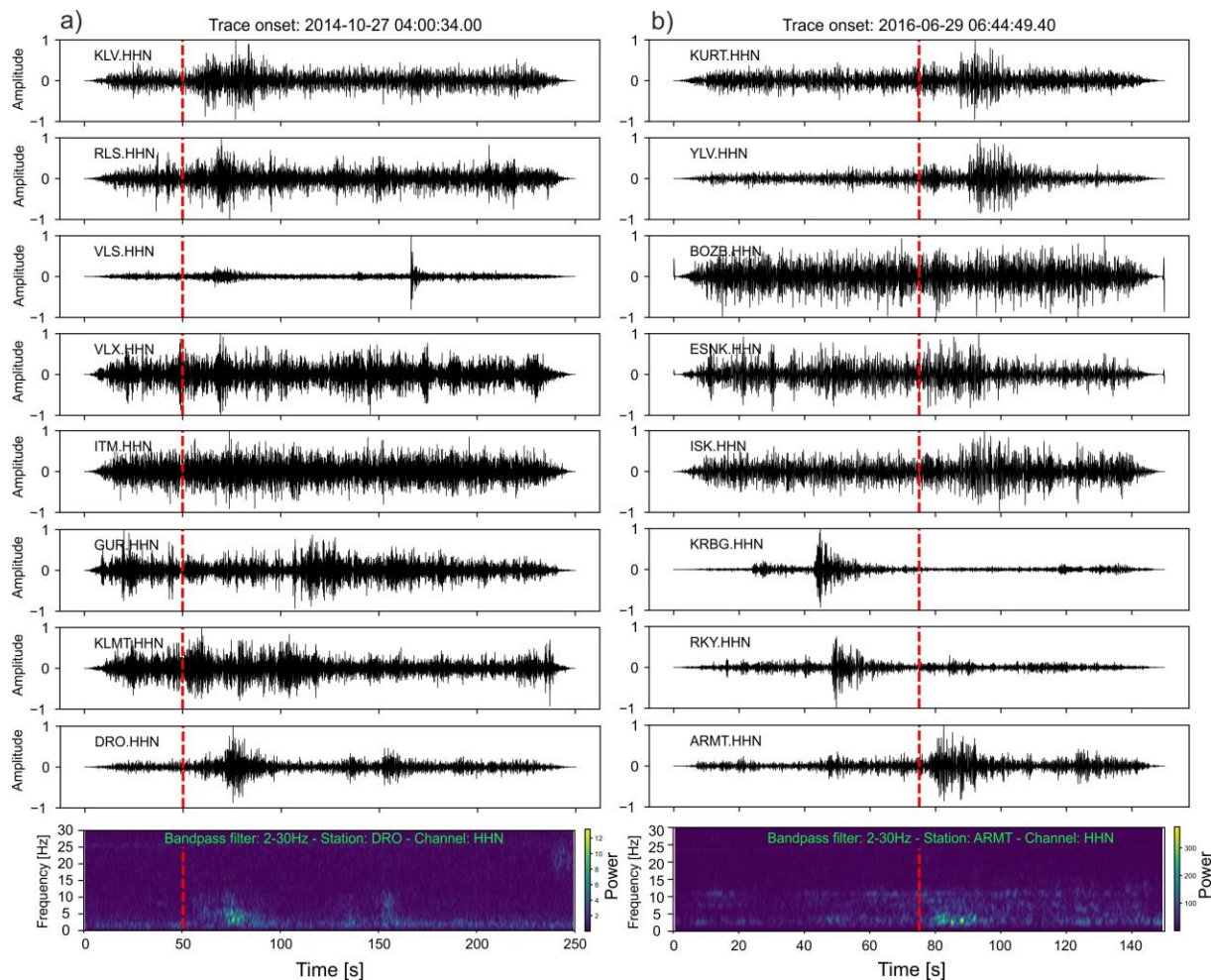


**Figure 5.** Example of detected signals using the automatic cross correlation method at the Hellenic Subduction Zone (a) and in the eastern Marmara Sea along the North Anatolian Fault (b). The red line shows the detection time of the signal which does not correspond to the origin time. The bottom panels show the spectrogram of the detected signals shown in the panels above them. The signals are detected by using half-overlapping windows of 300 sec and a cross correlation value of 0.6 at 5 or more channels at stations located <100 km apart. Amplitudes are normalized (-1, 1). All traces are bandpass filtered between 2-8 Hz. Station location is shown in Figure 1S.

## 422 5 Discussion

423 The most prominent worldwide reported examples of ambient and triggered tremor are  
 424 primarily limited to fault systems or plate bounding faults located along the Pacific rim (Wech  
 425 and Creager, 2008; Brown et al., 2009; Ide, 2012; Wech, 2016). The Oriente Fault in Cuba  
 426 represents, to date, the only exception (Peng et al., 2013) to the above correlation. The results  
 427 presented here suggest that the lack of deep tremor evidence outside of the Pacific rim point to a  
 428 requirement that specific conditions may be needed for tremor genesis. In the following, we

429 discuss similarities and differences between the Pacific and the Mediterranean regions to better  
430 understand the most relevant conditions for tremor genesis. Although the station coverage is less  
431 dense compared to some regions where tremor is observed, it is nevertheless sufficient to  
432 observe triggered tremor in the study regions in which we focus, should it occur. Triggered  
433 tremor has been recorded at stations more than 100 km apart (Peng et al., 2009), a significantly  
434 wider station spacing than used in all four study regions in this work. One limitation of the  
435 triggered tremor analysis could be the short time period of investigation, particularly in cases  
436 where hypothetical ETS episodes would have longer inter-event periods (for example, if they  
437 were to exceed 10 years in the other three regions). The relation between background and  
438 triggered tremor is still poorly understood (Chao et al., 2012a), however, many documented  
439 cases suggest that tremor is commonly triggered by low stress perturbations (slightly larger than,  
440 or similar to tidal stresses e.g. Thomas et al., 2009; Houston, 2015) in areas where ambient  
441 tremor occurs, and the time windows considered should be ample to detect triggered tremor. For  
442 instance, along the Simi Valley segment of the San Andreas Fault in southern California, where  
443 no unambiguous case of ambient tremor is documented, apparent triggering threshold are  
444 suggested to be much larger than those for the Parkfield–Cholame section of the San Andreas  
445 Fault ( $> \sim 12$  kPa and 2–3 kPa, respectively; Yang and Peng, 2013), where ambient tremor  
446 occurs. Another limitation could be the relatively low  $PGV_{\text{obs}}$  values recorded in our study  
447 regions with respect to circum-Pacific fault systems where tremor occurs, that lie closer to the  
448 sources of  $M > 7-7.5$  earthquakes. However, we note that the 0.1 cm/s threshold is exceeded  
449 during 4-5 events, or 3 events considering a 20 sec period, within each region (Fig. 3a-d), and the  
450 estimated dynamic stresses perturbations are  $> 9$  kPa. Therefore, many of what appear to be the  
451 important physical criteria associated with observed cases of triggering are met by the candidate  
452 mainshocks here. Thus, working on the assumption that the mainshocks generated stress  
453 perturbations sufficient to trigger tremor, in the following, we discuss possible causes of absence  
454 of tremor in the investigated subduction (5.1) and transform fault systems (5.2).

#### 455 5.1. Absence of tremor along the Calabrian and the Hellenic Arc

456 The most striking difference between the Pacific subduction zones and the Mediterranean  
457 subduction zones is arguably the age of the down-going plate (Fig. 1, Müller et al., 2008). In  
458 addition, relevant differences are represented by the accretionary prisms, with those in the

459 Mediterranean Sea being wider and thicker (Clift and Vannucchi, 2004), and by the convergence  
460 rates, which are on average lower within the Mediterranean basin (Matthews et al., 2016).

461 The age of the down-going slab controls the thermal state of subducting plate with older  
462 slabs being colder and younger slabs being warmer (Peacock and Wang, 1999). Young slabs  
463 dehydrate at shallower depths while older slabs dehydrate at greater depth, resulting in  
464 significant differences in subduction dynamics (Peacock and Wang, 1999). For instance, in  
465 warmer subduction zones (e.g. Cascadia, Mexico, Nankai), the brittle-plastic transition (assumed  
466 to be near the 350° C isotherm) occurs at shallower depths (Fig. 2a-b; Peacock and Wang, 1999),  
467 and the mantle wedge corner is more hydrated (Abers et al., 2017) relative to older subduction  
468 zones (Fig. 6). Thermal models for the Hellenic subduction zone show that the 350° isotherm lies  
469 at ~60 km depth (Bocchini et al., 2018; Halpaap et al., 2019), well-below the down-dip limit of  
470 the seismogenic zone south of Crete and the intersection between the down-going plate and the  
471 overriding plate Moho (Fig. 6b). Although the intersection between the upper-plate Moho and  
472 the down-going slab south of Crete is not well-defined, it is not located far from the southern  
473 coastline of the Island (Bohnhoff et al., 2001). Hence, the absence of deep tremor is not  
474 surprising if we expect it to occur when the down-dip limit of the megathrust is shallower than  
475 the slab upper-plate Moho intersection depth (Fig 6a; Gao and Wang, 2017).

476 A similar situation can be hypothesized for the Calabrian arc, due to the similar age of the  
477 subducting slab and its intersection with the upper-plate Moho at ~25 km. In fact, thermal  
478 models suggest that the 350° isotherm occurs at depths much greater than 25 km (Fig. 2b)  
479 (Syracuse et al., 2010). However, although not in oceanic crust as old as the Mediterranean  
480 oceanic lithosphere (>220-230 Ma), tremor does occur at subduction zones where the down-  
481 going slab is older than 100 Ma. Examples are the Hikurangi trench in New Zealand (Ide, 2012)  
482 and the NE Japan Trench (Nishikawa et al., 2019), where both have common, unique conditions  
483 that may prime them for the occurrence of tremor. For instance, deep tremorigenic conditions in  
484 New Zealand are explained to be consequence of the high frictional heating along the megathrust  
485 that shifts the brittle-plastic transition at depths shallower than that of the upper-plate Moho  
486 (Yabe et al., 2014; Gao and Wang, 2017). In NE Japan, tremor occurs at seismogenic depths  
487 where tremorigenic conditions are promoted by frictional heterogeneities likely induced by pore  
488 fluid changes, sea floor roughness, and/or fracturing of the upper-plate (Nishikawa et al., 2019).  
489 We note that in the latter case, tremor at seismogenic depths may be viewed as a special case, as

490 it does not fulfill the definition of deep tremor outlined at the beginning of the paper. In addition,  
491 we note another unique example involving the subduction of fluid rich sediments, which is also  
492 invoked to explain the deep tremor sources at the eastern termination of the Alaskan subduction  
493 zone (at 60-80 km), to date the deepest, well recorded example of tremor worldwide (Wech,  
494 2016).

495         Very likely there are no anomalous physical conditions present at the Hellenic and  
496 Calabrian subduction zones that would be able to create a tremorigenic environment. For instance  
497 heat flow values offshore south of Crete (20-30 mW/m<sup>2</sup>; Eckstein, 1978), as well as in  
498 continental Calabria (~40 mW/m<sup>2</sup>; Loddo et al., 1973) are comparatively low and consistent  
499 with the age of the subducting slab, hence excluding the presence of a warm, strong megathrust  
500 as in the case of Hikurangi (Gao and Wang, 2014). The mantle wedge corner at both subduction  
501 zones is expected to be poorly hydrated due to the old nature of the subducting lithosphere  
502 (Abers et al., 2017; Halpaap et al., 2019). In addition, the mantle wedge corner beneath Crete is  
503 expected to be poorly hydrated because the current subduction configuration was reached only  
504 15-20 Ma ago (Thomson et al., 1999). It has been proposed that temperature-dependent silica  
505 precipitation by upward migrating fluid derived from the down-going slab, by reducing  
506 permeability in the forearc crust, favor fluid overpressures and therefore deep tremorigenic  
507 conditions (Audet and Bürgmann, 2014). The potential for silica-rich fluids exists in subduction  
508 zones where conditions favor high temperatures (Manning, 1997) and it is greatly enhanced by  
509 complete serpentinization of the mantle wedge corner (Audet and Bürgmann, 2014). At both the  
510 analyzed subduction zones such conditions are not met.

511         The role that the very thick layer of sediments on the down-going plate could play is not  
512 easy to address. ETS episodes are observed in erosional (e.g. Mexico) as well as in accretional  
513 (e.g. Cascadia or Nankai) subducting margins (Clift and Vannucchi, 2004). Sediments are water  
514 rich and can carry it down, up to 200 km depth. However, they release a considerably smaller  
515 amount of water than other slab dehydration sources (van Keken et al., 2011), therefore are not  
516 expected to significantly contribute to the hydration of the mantle wedge corner.

517         With respect to the low geodetic locking depth at both the Hellenic (Vernant et al., 2014)  
518 and the Calabrian subduction zones (Pérouse et al., 2012), previous studies suggest that variation  
519 of geodetic locking is not correlated to the distribution of deep tremor (Brown et al., 2013).

520 Therefore, we do not consider the low geodetic locking as relevant to prevent the occurrence of  
521 tremor. At the Calabrian Arc, the very low convergence rate may affect the occurrence of tremor,  
522 as tremor is not observed elsewhere fault systems moving slower than 5 mm/yr. We note the  
523 convergence rates at the Hellenic subduction zone are comparable to those of the slower  
524 subduction margins where tremor is observed (e.g. Cascadia, Hikurangi), therefore should not  
525 prevent tremor occurrence.

526 This study does not exclude that tremor could occur above the up-dip limit of the  
527 seismogenic zone. The presence of widespread mud volcanos between the backstop and the  
528 accretionary wedges of both the Calabrian (Panieri et al., 2013) and Hellenic (Huguen et al.,  
529 2001) subduction zones hints at large amounts of fluids released by sediments. High pore fluid  
530 pressure could promote tremorigenic conditions above the up-dip limit of the seismogenic zone  
531 (Saffer and Wallace, 2015). As already stated, we do not observe any coherent tremor-like signal  
532 during surface wave shaking of large mainshocks which suggests the absence of such signals  
533 also from different locations other than the down-dip limit of the seismogenic zone. However, as  
534 in case of Crete, the up-dip limit of the seismogenic zone is located ~50-60 km to the south of  
535 the island (Meier et al., 2004), therefore it could be difficult to observe low amplitude signals at  
536 land stations. To rule out or confirm the occurrence of tremor at shallower depths than those  
537 expected for the ETS zone, the deployment of dense Ocean Bottom Seismometer networks, as  
538 for instance in NE Japan (Nishikawa et al., 2019), would be needed.

539 Very recently SSEs have been found at the down-dip limit of the seismogenic zone, at  
540 depths of 20-40 km beneath western Peloponnese (Mouslopoulou et al., 2020) leaving open the  
541 possibility that they may even occur along other segments of the Hellenic Subduction Zone  
542 (Saltogianni et al., 2020). The limitation of publicly available geodetic data may have prevented  
543 their detection elsewhere. The duration, location and the equivalent moment magnitude released  
544 are consistent with those of long-term SSEs (Obara and Kato, 2016). Long-term SSEs are  
545 suggested to be manifestation of semi-brittle more towards viscous behavior and are not  
546 commonly associated with tremor (Gao and Wang, 2017). In contrast, semi-brittle more towards  
547 brittle behavior is invoked to explain ETS episodes (Gao and Wang, 2017). The observations of  
548 long-term SSEs at the Hellenic Subduction Zone may suggest the more widespread conditions  
549 for long-term SSEs occurrence with respect to that required for ETS episodes (Bürgmann, 2018).

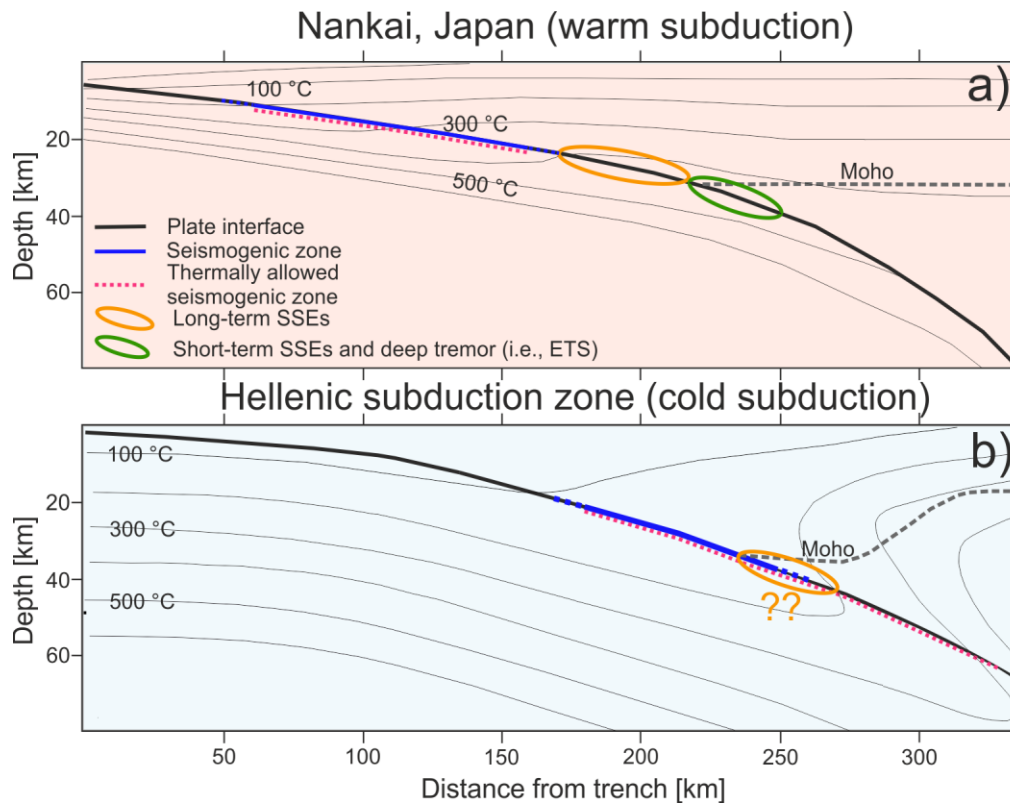


**Figure 6.** Sketch comparing typical slip behavior in a (a) warm subduction zone and a (b) cold subduction zone. (a) Cross-section along the Nankai trench (Japan) adapted from Gao and Wang (2017). (b) Cross-section across Crete using slab geometry and thermal structure from half-space cooling model in Bocchini et al. (2018). Upper-plate Moho depth in subfigure b from available active and passive seismological studies (Bohnhoff et al., 2001; Meier et al., 2007).

550 5.2. Absence of tremor along the Kefalonia Transform Fault and North Anatolia Fault in  
551 the Sea of Marmara

552 Of the documented cases of tremor along transform margins, the most well-established  
553 examples are for the Parkfield-Cholame segment of the San Andreas Fault (Nadeau and Dolenc,  
554 2005; Peng et al., 2009, Shelly, 2017). The occurrence of tremor in the Parkfield-Cholame area is  
555 interpreted to be related to the presence of remnants of partially serpentinized mantle wedge  
556 from a former subduction zone (Kirby et al., 2014). The frequency of tremor episodes  
557 significantly decreases towards NW (Calaveras) and SE (San Jacinto) along the SAF (Gomberg  
558 et al., 2008; Peng et al., 2009) enhancing the primary control exerted by the water reservoir  
559 beneath the Parkfield-Cholame segment. Although less frequent, deep tremor activity beneath  
560 the Alpine Fault in New Zealand is also related to the presence of high pore fluid pressures  
561 (Wech et al., 2012). Along the Kefalonia Fault and the North Anatolian Fault segment in the Sea  
562 of Marmara, such a fluid source is possibly missing and/or do not exist the conditions to create

563 high fluid pressures to promote tremorgenesis. Our results along the North Anatolian Fault are  
564 consistent with those of Pfohl et al. (2015) that found no unambiguous evidence for triggered or  
565 ambient tremor along the central segment of the North Anatolian Fault. In addition, the  
566 transtensional regime in the Sea of Marmara may also not be favorable for tremor occurrence, as  
567 most observations of tremor occur along compressive or transform/transpressive margins (Fig.  
568 1). While the Kefalonia Transform Fault exhibits transpressional deformation like the Alpine and  
569 San Andreas Faults, it shows a different tectonic evolution. For example, it is not located along a  
570 former suture zone and it is much younger, with less accumulated displacement (van Hinsbergen  
571 et al., 2006). Furthermore, the seismogenic layer and the Moho depths do not occur at anomalous  
572 depths at either the Kefalonia Transform Fault as well as at the Çınarcık segment of the North  
573 Anatolian Fault (section 2.1 and section 2.4) that could hint at significantly high or low  
574 temperature gradients.

575 The absence of triggered tremor in the eastern Marmara Sea agrees with the absence of  
576 LFE/tremor activity accompanying the ~50-daylong SSE along the Çınarcık fault (Martínez-  
577 Garzón et al., 2019). The absence of ambient tremor would imply that the SSE could have either  
578 occurred at shallow depth, consistently to adjacent segments of the North Anatolian Fault (Aslan  
579 et al., 2019; Rousset et al., 2016) or if at the down-dip limit of the seismogenic zone, to exhibit  
580 similar characteristics of the long-term SSEs that are observed to be not strongly correlated with  
581 the occurrence of tremor (Husker et al., 2012; Obara, 2011). The occurrence of shallow SSE  
582 along adjacent segments of the North Anatolian Fault would support the shallow origin of the  
583 signal.

## 584 **6 Conclusions**

585 We find no unambiguous evidence for triggered deep tremor at the Hellenic Subduction  
586 Zone, beneath Crete, at the Calabrian Subduction Zone, at the Kefalonia Transform Fault, and at  
587 the North Anatolian Fault, in the eastern Marmara Sea, during the passage of surface waves of  
588 16-18 teleseismic events between 2010 and 2020. Furthermore, we find no unambiguous  
589 examples of LFE/tremor activity accompanying the SSE in the eastern Marmara Sea and the two  
590 SSEs beneath Peloponnese, along the western segment of the Hellenic Subduction Zone. The  
591 absence of tremor along the North Anatolian Fault agrees with the findings from a previous  
592 study. The absence of triggered tremor, strengthened by the absence of ambient tremor during

593 SSE episodes, suggests the absence of favorable physical conditions for a deep ETS zone in the  
594 central-eastern Mediterranean basin. The results confirm the significant influence of the slab  
595 thermal structure on the occurrence of deep tremor in subduction zones. The very old and cold  
596 slabs at the Calabrian and Hellenic subduction zones do not favor tremorgenesis. The possible  
597 absence of fluid sources, able to promote elevated pore fluid pressures at the base of the  
598 seismogenic layers at the Kefalonia and North Anatolian transform faults could explain the  
599 absence of tremor. In addition, the transtensional regime within the Çınarcık basin, in the eastern  
600 Sea of Marmara, does not seem favorable to the generation of tremor. The absence of  
601 LFEs/tremor activity accompanying the SSE along the Çınarcık Fault in the eastern Sea of  
602 Marmara would suggest that the detected ~50-daylong SSE occurred either at shallow depths in  
603 agreement with observations from adjacent segments, or that, if deep, could be classified as long-  
604 term SSE. The depth range, duration, and absence of tremor during the SSEs along the western  
605 segment of the Hellenic Subduction Zone are also consistent with those of long-term SSEs  
606 observed elsewhere. The absence of deep tremor indicate the more widespread conditions for the  
607 occurrence of long-term SSEs, likely a manifestation of semi-brittle more towards viscous  
608 behavior, compared to that suggested for ETS that require a restoration of a brittle or semi-brittle  
609 regime at depths where under normal condition rocks would deform viscously.

#### 610 **Acknowledgments, Samples, and Data**

611 G.M.B has been funded with Ruhr Uuniversity of Bochum new faculty startup funds awarded to  
612 R.M.H.. P.M-G. acknowledges funding from the Helmholtz Young Investigators Group:  
613 SAIDAN (VH-NG-1323). We are grateful to the Institute of Geodynamics of the National  
614 Observatory of Athens (NOA, Greece) and all partners of the Hellenic Unified Seismic Network,  
615 including the University of Patra, University of Thessaloniki and University of Athens, to the  
616 Technological Educational Institute of Crete (Greece), to INGV (Italy), to KOERI (Turkey)  
617 technical staff for the installation and maintenance of seismic networks and for publicly sharing  
618 data. Data from such networks used in this study are freely accessible from EIDA database.  
619 Thanks to the Turkish Disaster and Emergency Management Presidency (AFAD) in Ankara for  
620 providing waveform data from the GONAF observatory. Access to the GONAF and PIREs  
621 networks is granted upon request to Marco Bohnhoff (GFZ). Many thanks to Yajing Liu for her  
622 constructive comments on a draft of the manuscript and to Satoshi Ide for having shared the  
623 envelope cross-correlation code for ambient tremor detection. Figures were realized using the  
624 Global Mapping Tool (Wessel et al., 2013) and matplotlib. Waveform data processing was  
625 performed with Obspy.  
626

627 **References**

- 628 Abers, G.A., Van Keken, P.E., & Hacker, B.R. (2017), The cold and relatively dry nature of  
629 mantle forearcs in subduction zones. *Nature Geosciences*. <https://doi.org/10.1038/ngeo2922>
- 630 Aiken, C., Peng, Z., & Chao, K. (2013), Tremors along the Queen Charlotte Margin triggered by  
631 large teleseismic earthquakes. *Geophysical Research Letters*.  
632 <https://doi.org/10.1002/grl.50220>
- 633 Aki, K., & Richards, P.G. (2002), Quantitative seismology.
- 634 Armijo, R., Meyer, B., Navarro, S., King, G., & Barka, A. (2002), Asymmetric slip partitioning  
635 in the sea of Marmara pull-apart: A clue to propagation processes of the North Anatolian  
636 Fault? *Terra Nova*. <https://doi.org/10.1046/j.1365-3121.2002.00397.x>
- 637 Aslan, G., Lasserre, C., Cakir, Z., Ergintav, S., Özarpaci, S., Dogan, U., Bilham, R., & Renard,  
638 F. (2019), Shallow Creep Along the 1999 Izmit Earthquake Rupture (Turkey) From GPS  
639 and High Temporal Resolution Interferometric Synthetic Aperture Radar Data (2011–2017).  
640 *Journal Geophysical Research: Solid Earth*. <https://doi.org/10.1029/2018JB017022>
- 641 Audet, P., Bostock, M.G., Christensen, N.I., & Peacock, S.M. (2009), Seismic evidence for  
642 overpressured subducted oceanic crust and megathrust fault sealing. *Nature*, 457, 76–78.  
643 <https://doi.org/10.1038/nature07650>
- 644 Audet, P., & Bürgmann, R. (2014), Possible control of subduction zone slow-earthquake  
645 periodicity by silica enrichment. *Nature*. <https://doi.org/10.1038/nature13391>
- 646 Audet, P., & Kim, Y.H. (2016), Teleseismic constraints on the geological environment of deep  
647 episodic slow earthquakes in subduction zone forearcs: A review. *Tectonophysics*.  
648 <https://doi.org/10.1016/j.tecto.2016.01.005>
- 649 Becker, D., & Meier, T. (2010), Seismic slip deficit in the southwestern forearc of the hellenic  
650 subduction zone. *Bulletin of the Seismological Society of America*, 100, 325–342.  
651 <https://doi.org/10.1785/0120090156>
- 652 Bocchini, G.M., Brüstle, A., Becker, D., Meier, T., van Keken, P.E., Ruscic, M., Papadopoulos,  
653 G.A., Rische, M., & Friederich, W. (2018), Tearing, segmentation, and backstepping of  
654 subduction in the Aegean: New insights from seismicity. *Tectonophysics*, 734–735, 96–118.  
655 <https://doi.org/10.1016/j.tecto.2018.04.002>
- 656 Bockholt, B.M., Langston, C.A., Horton, S., Withers, M., & Deshon, H.R. (2014), Mysterious  
657 tremor-like signals seen on the reelfoot fault, Northern Tennessee. *Bulletin Seismological*  
658 *Society of America*. <https://doi.org/10.1785/0120140030>
- 659 Bohnhoff, M., Dresen, G., Ceken, U., Kadirioglu, F.T., Kartal, R.F., Kilic, T., Nurlu, M., Yanik,  
660 K., Acarel, D., Bulut, F., Ito, H., Johnson, W., Malin, P.E., & Mencin, D. (2017), GONAF -  
661 The borehole geophysical observatory at the North Anatolian Fault in the eastern Sea of  
662 Marmara. *Scientific Drilling*. <https://doi.org/10.5194/sd-22-19-2017>

- 663 Bohnhoff, M., Makris, J., Papanikolaou, D., & Stavrakakis, G. (2001), Crustal investigation of  
 664 the Hellenic subduction zone using wide aperture seismic data. *Tectonophysics*, 343, 239–  
 665 262. [https://doi.org/10.1016/S0040-1951\(01\)00264-5](https://doi.org/10.1016/S0040-1951(01)00264-5)
- 666 Bohnhoff, M., Martínez-Garzón, P., Bulut, F., Stierle, E., & Ben-Zion, Y. (2016), Maximum  
 667 earthquake magnitudes along different sections of the North Anatolian fault zone.  
 668 *Tectonophysics*. <https://doi.org/10.1016/j.tecto.2016.02.028>
- 669 Brown, J.R., Beroza, G.C., Ide, S., Ohta, K., Shelly, D.R., Schwartz, S.Y., Rabbel, W., Thorwart,  
 670 M., & Kao, H. (2009), Deep low-frequency earthquakes in tremor localize to the plate  
 671 interface in multiple subduction zones. *Geophysical Research Letters*.  
 672 <https://doi.org/10.1029/2009GL040027>
- 673 Brown, J.R., Prejean, S.G., Beroza, G.C., Gombert, J.S., & Haeussler, P.J. (2013), Deep low-  
 674 frequency earthquakes in tectonic tremor along the Alaska-Aleutian subduction zone.  
 675 *Journal of Geophysical Research: Solid Earth*. <https://doi.org/10.1029/2012JB009459>
- 676 Bürgmann, R., (2018), The geophysics, geology and mechanics of slow fault slip. *Earth and*  
 677 *Planetary Science Letters*. <https://doi.org/10.1016/j.epsl.2018.04.062>
- 678 Carafa, M.M.C., Kastelic, V., Bird, P., Maesano, F.E., & Valensise, G. (2018), A “Geodetic  
 679 Gap” in the Calabrian Arc: Evidence for a Locked Subduction Megathrust?. *Geophysical*  
 680 *Research Letters*. <https://doi.org/10.1002/2017GL076554>
- 681 Carton, H., Singh, S.C., Hirn, A., Bazin, S., de Voogd, B., Vigner, A., Ricolleau, A., Cetin, S.,  
 682 Oçakoğlu, N., Karakoç, F., & Sevilgen, V. (2007), Seismic imaging of the three-  
 683 dimensional architecture of the Çınarcık Basin along the North Anatolian Fault. *Journal of*  
 684 *Geophysical Research: Solid Earth*. <https://doi.org/10.1029/2006JB004548>
- 685 Chamberlain, C.J., Hopp, C.J., Boese, C.M., Warren-Smith, E., Chambers, D., Chu, S.X.,  
 686 Michailos, K., & Townend, J. (2018), EQcorrscan: Repeating and near-repeating earthquake  
 687 detection and analysis in python. *Seismological Research Letters*.  
 688 <https://doi.org/10.1785/0220170151>
- 689 Chao, K., Peng, Z., Fabian, A., & Ojha, L. (2012a), Comparisons of triggered tremor in  
 690 California. *Bulletin of the Seismological Society of America*.  
 691 <https://doi.org/10.1785/0120110151>
- 692 Chao, K., Peng, Z., Gonzalez-Huizar, H., Aiken, C., Enescu, B., Kao, H., Velasco, A.A., Obara,  
 693 K., & Matsuzawa, T. (2013), A Global search for triggered tremor following the 2011 Mw  
 694 9.0 Tohoku earthquake. *Bulletin of the Seismological Society of America*.  
 695 <https://doi.org/10.1785/0120120171>
- 696 Chao, K., Peng, Z., Wu, C., Tang, C.C., & Lin, C.H. (2012b), Remote triggering of non-volcanic  
 697 tremor around Taiwan. *Geophysical Journal International*. <https://doi.org/10.1111/j.1365-246X.2011.05261.x>
- 699 Clift, P., & Vannucchi, P. (2004), Controls on tectonic accretion versus erosion in subduction

- 700 zones: Implications for the origin and recycling of the continental crust. *Reviews*  
 701 *Geophysics*. <https://doi.org/10.1029/2003RG000127>
- 702 de Voogd, B., Truffert, C., Chamot-Rooke, N., Huchon, P., Lallemand, S., Le Pichon, X., (1992),  
 703 Two-ship deep seismic soundings in the basins of the Eastern Mediterranean Sea (Pasiphae  
 704 cruise). *Geophysical Journal International*. [https://doi.org/10.1111/j.1365-](https://doi.org/10.1111/j.1365-246X.1992.tb00116.x)  
 705 [246X.1992.tb00116.x](https://doi.org/10.1111/j.1365-246X.1992.tb00116.x)
- 706 Dickinson, W.R., & Wernicke, B.P. (1997), Reconciliation of San Andreas slip discrepancy by a  
 707 combination of interior basin and range extension and transrotation near the coast. *Geology*.  
 708 [https://doi.org/10.1130/0091-7613\(1997\)025<0663:ROSASD>2.3.CO;2](https://doi.org/10.1130/0091-7613(1997)025<0663:ROSASD>2.3.CO;2)
- 709 Eckstein, Y. (1978), Review of heat flow data from the eastern Mediterranean region. *Pure*  
 710 *Applied Geophysics*, 117, 150–159.
- 711 Faccenna, C., Becker, T.W., Auer, L., Billi, A., Boschi, L., Brun, J.P., Capitanio, F.A.,  
 712 Funiciello, F., Horvath, F., Jolivet, L., Piromallo, C., Royden, L., Rossetti, F., & Serpelloni,  
 713 E. (2014), Mantle dynamics in the Mediterranean. *Reviews Geophysics*, 52, 283–332.  
 714 <https://doi.org/10.1002/2013RG000444>.Received
- 715 Faccenna, C., Funiciello, F., Giardini, D., & Lucente, P. (2001), Episodic back-arc extension  
 716 during restricted mantle convection in the Central Mediterranean. *Earth and Planetary*  
 717 *Science Letters*. [https://doi.org/10.1016/S0012-821X\(01\)00280-1](https://doi.org/10.1016/S0012-821X(01)00280-1)
- 718 Fry, B., Chao, K., Bannister, S., Peng, Z., & Wallace, L. (2011), Deep tremor in New Zealand  
 719 triggered by the 2010 Mw8.8 Chile earthquake. *Geophysical Research Letters*.  
 720 <https://doi.org/10.1029/2011GL048319>
- 721 Gao, X., & Wang, K. (2014), Strength of stick-slip and creeping subduction megathrusts from  
 722 heat flow observations. *Science* (80-. ). <https://doi.org/10.1126/science.1255487>
- 723 Gao, X., & Wang, K. (2017), Rheological separation of the megathrust seismogenic zone and  
 724 episodic tremor and slip. *Nature*. <https://doi.org/10.1038/nature21389>
- 725 GFZ Potsdam, BU-Kandilli (2006), Prince Islands Real-time Earthquake monitoring System.  
 726 International Federation of Digital Seismograph Networks. Dataset/Seismic Network.  
 727 <https://doi.org/10.7914/SN/PZ>
- 728 Ghosh, A., Vidale, J.E., Peng, Z., Creager, K.C., Houston, H. (2009a), Complex nonvolcanic  
 729 tremor near Parkfield, California, triggered by the great 2004 Sumatra earthquake. *Journal*  
 730 *of Geophysical Research: Solid Earth*. <https://doi.org/10.1029/2008JB006062>
- 731 Ghosh, A., Vidale, J.E., Sweet, J.R., Creager, K.C., & Wech, A.G. (2009b), Tremor patches in  
 732 Cascadia revealed by seismic array analysis. *Geophysical Research Letters*.  
 733 <https://doi.org/10.1029/2009GL039080>
- 734 Gomberg, J., Rubinstein, J.L., Peng, Z., Creager, K.C., Vidale, J.E., & Bodin, P. (2008),  
 735 Widespread triggering of nonvolcanic tremor in California. *Science* (80-. ).

- 736 <https://doi.org/10.1126/science.1149164>
- 737 Granot, R. (2016), Palaeozoic oceanic crust preserved beneath the eastern Mediterranean. *Nature*  
738 *Geoscience*, 9, 701–705. <https://doi.org/10.1038/ngeo2784>
- 739 Guidoboni, E., & Comastri, A. (2005), Catalogue of earthquakes and tsunamis in the  
740 Mediterranean area from the 11th to the 15th century. Rome : Istituto nazionale di geofisica  
741 e vulcanologia.
- 742 Halpaap, F., Rondenay, S., Perrin, A., Goes, S., Ottemöller, L., Austrheim, H., Shaw, R., &  
743 Eeken, T. (2019), Earthquakes track subduction fluids from slab source to mantle wedge  
744 sink. *Science Advances*. <https://doi.org/10.1126/sciadv.aav7369>
- 745 Houston, H. (2015), Low friction and fault weakening revealed by rising sensitivity of tremor to  
746 tidal stress. *Nature Geoscience*. <https://doi.org/10.1038/ngeo2419>
- 747 Huguen, C., Mascle, J., Chaumillon, E., Woodside, J.M., Benkhelil, J., Kopf, A., & Volkonskaia,  
748 A. (2001), Deformational styles of the Eastern Mediterranean ridge and surroundings from  
749 combined swath mapping and seismic reflection profiling. *Tectonophysics*, 343, 21–47.  
750 [https://doi.org/10.1016/S0040-1951\(01\)00185-8](https://doi.org/10.1016/S0040-1951(01)00185-8)
- 751 Husker, A.L., Kostoglodov, V., Cruz-Atienza, V.M., Legrand, D., Shapiro, N.M., Payero, J.S.,  
752 Campillo, M., & Huesca-Pérez, E. (2012), Temporal variations of non-volcanic tremor  
753 (NVT) locations in the Mexican subduction zone: Finding the NVT sweet spot.  
754 *Geochemistry, Geophysics and Geosystems*. <https://doi.org/10.1029/2011GC003916>
- 755 Ide, S. (2010), Striations, duration, migration and tidal response in deep tremor. *Nature*.  
756 <https://doi.org/10.1038/nature09251>
- 757 Ide, S. (2012), Variety and spatial heterogeneity of tectonic tremor worldwide. *Journal of*  
758 *Geophysical Research: Solid Earth*. <https://doi.org/10.1029/2011JB008840>
- 759 ISC, International Seismological Centre (2020), On-line Bulletin.  
760 <https://doi.org/10.31905/D808B830>
- 761 Ito, Y., Obara, K., Shiomi, K., Sekine, S., & Hirose, H. (2007), Slow earthquakes coincident with  
762 episodic tremors and slow slip events. *Science* (80-. ).  
763 <https://doi.org/10.1126/science.1134454>
- 764 Jenkins, J., Stephenson, S.N., Martínez-Garzón, P., Bohnhoff, M., & Nurlu, M. (2020), Crustal  
765 thickness variation across the Sea of Marmara region, NW Turkey: a reflection of modern  
766 and ancient tectonic processes. *Tectonics*. <https://doi.org/10.1029/2019TC005986>
- 767 Kennett, B.L.N., & Engdahl, E.R. (1991), Traveltimes for global earthquake location and phase  
768 identification. *Geophysical Journal International*. [https://doi.org/10.1111/j.1365-](https://doi.org/10.1111/j.1365-246X.1991.tb06724.x)  
769 [246X.1991.tb06724.x](https://doi.org/10.1111/j.1365-246X.1991.tb06724.x)
- 770 Kim, M.J., Schwartz, S.Y., & Bannister, S. (2011), Non-volcanic tremor associated with the

- 771 March 2010 Gisborne slow slip event at the Hikurangi subduction margin, New Zealand.  
772 *Geophysical Research Letters*. <https://doi.org/10.1029/2011GL048400>
- 773 Kirby, S.H., Wang, K., & Brocher, T.M. (2014), A large mantle water source for the northern  
774 san andreas fault system: A ghost of subduction past. *Earth, Planets and Space*.  
775 <https://doi.org/10.1186/1880-5981-66-67>
- 776 Kodaira, S., Iidaka, T., Kato, A., Park, J.O., Iwasaki, T., & Kaneda, Y. (2004), High pore fluid  
777 pressure may cause silent slip in the Nankai Trough. *Science* (80-. ).  
778 <https://doi.org/10.1126/science.1096535>
- 779 Lay, T., & Wallace, T.C. (1995), *Modern global seismology*. Elsevier.
- 780 Le Pichón, X., Şeng ÖR, A.M.C., Kende, J., İmren, C., Henry, P., Grail, C., & Karabulut, H.  
781 (2016), Propagation of a strike-slip plate boundary within an extensional environment: The  
782 westward propagation of the North Anatolian fault. *Canadian Journal of Earth Sciences*.  
783 <https://doi.org/10.1139/cjes-2015-0129>
- 784 Loddo, M., Mongelli, F., & Roda, C. (1973), Heat flow in Calabria, Italy. *Nature Physics*  
785 *Science*, 244, 91–92.
- 786 Louvari, E., Kiratzi, A.A., & Papazachos, B.C. (1999), The Cephalonia Transform Fault and its  
787 extension to western Lefkada Island (Greece). *Tectonophysics*, 308, 223–236.  
788 [https://doi.org/10.1016/S0040-1951\(99\)00078-5](https://doi.org/10.1016/S0040-1951(99)00078-5)
- 789 Maesano, F.E., Tiberti, M.M., & Basili, R. (2017), The Calabrian Arc: Three-dimensional  
790 modelling of the subduction interface. *Scientific Reports*. <https://doi.org/10.1038/s41598-017-09074-8>
- 792 Malin, P.E., Bohnhoff, M., Blümle, F., Dresen, G., Martínez-Garzón, P., Nurlu, M., Ceken, U.,  
793 Kadirioğlu, F.T., Kartal, R.F., Kilic, T., & Yanik, K. (2018), Microearthquakes preceding a  
794 M4.2 Earthquake Offshore Istanbul. *Scientific Reports*. <https://doi.org/10.1038/s41598-018-34563-9>
- 796 Manning, C.E. (1997), Coupled Reaction and Flow in Subduction Zones: Silica Metasomatism in  
797 the Mantle Wedge. In: *Fluid Flow and Transport in Rocks*. [https://doi.org/10.1007/978-94-009-1533-6\\_8](https://doi.org/10.1007/978-94-009-1533-6_8)
- 799 Martínez-Garzón, P., Bohnhoff, M., Mencin, D., Kwiatek, G., Dresen, G., Hodgkinson, K.,  
800 Nurlu, M., Kadirioğlu, F.T., & Kartal, R.F. (2019), Slow strain release along the eastern  
801 Marmara region offshore Istanbul in conjunction with enhanced local seismic moment  
802 release. *Earth and Planetary Science Letters*. <https://doi.org/10.1016/j.epsl.2019.01.001>
- 803 Martínez-Garzón, P., Heidbach, O., & Bohnhoff, M. (2020), Contemporary stress and strain field  
804 in the Mediterranean from stress inversion of focal mechanisms and GPS data.  
805 *Tectonophysics*, 774, 228286.
- 806 Matthews, K.J., Maloney, K.T., Zahirovic, S., Williams, S.E., Seton, M., & Müller, R.D. (2016),

- 807 Global plate boundary evolution and kinematics since the late Paleozoic. *Global and*  
808 *Planetary Change*. <https://doi.org/10.1016/j.gloplacha.2016.10.002>
- 809 McClusky, S., Balassanian, S., Barka, A., Demir, C., Ergintav, S., Georgiev, I., Gurkan, O.,  
810 Hamburger, M., Hurst, K., Kahle, H., Kastens, K., Kekelidze, G., King, R., Kotzev, V.,  
811 Lenk, O., Mahmoud, S., Mishin, A., Nadariya, M., Ouzounis, A., Paradissis, D., Peter, Y.,  
812 Prilepin, M., Reilinger, R., Sanli, I., Seeger, H., Tealeb, A., Toksöz, M.N., & Veis, G.  
813 (2000), Global Positioning System constraints on plate kinematics and dynamics in the  
814 eastern Mediterranean and Caucasus. *Journal of Geophysical Research: Solid Earth*, 105,  
815 5695–5719. <https://doi.org/10.1029/1999JB900351>
- 816 Meier, T., Becker, D., Endrun, B., Rische, M., Bohnhoff, M., Stöckhert, B., & Harjes, H.-P.  
817 (2007), A model for the Hellenic subduction zone in the area of Crete based on  
818 seismological investigations, in: Taymaz, T., Yilmaz, Y., Dilek, Y. (Eds.), *The Geodynamic*  
819 *of the Aegean and Anatolia. Geological Society, London, Special Publications*, 183–199.  
820 <https://doi.org/10.1144/SP291.9>
- 821 Meier, T., Rische, M., Endrun, B., Vafidis, A., & Harjes, H.-P. (2004), Seismicity of the Hellenic  
822 subduction zone in the area of western and central Crete observed by temporary local  
823 seismic networks. *Tectonophysics*, 383, 149–169.  
824 <https://doi.org/10.1016/j.tecto.2004.02.004>
- 825 Miyazawa, M., & Brodsky, E.E. (2008), Deep low-frequency tremor that correlates with passing  
826 surface waves. *Journal of Geophysical Research: Solid Earth*.  
827 <https://doi.org/10.1029/2006JB004890>
- 828 Miyazawa, M., Brodsky, E.E., & Mori, J. (2008), Learning from dynamic triggering of low-  
829 frequency tremor in subduction zones. *Earth, Planets and Space*.  
830 <https://doi.org/10.1186/BF03352858>
- 831 Mouslopoulou, V., Bocchini, G.M., Cesca, S., Saltogianni, V., Bedford, J.R., Petersen, G.M.,  
832 Gianniou, M., & Oncken, O. (2020), Earthquake-swarms, slow-slip and fault-interactions at  
833 the western-end of the Hellenic Subduction System precede the Mw 6.9 Zakynthos  
834 Earthquake, Greece. *Earth and Space Science Open Archive*.  
835 <https://doi.org/10.1002/essoar.10503389.1>
- 836 Müller, R.D., Sdrolias, M., Gaina, C., & Roest, W.R. (2008), Age, spreading rates, and spreading  
837 asymmetry of the world's ocean crust. *Geochemistry, Geophys. Geosystems*, 9.  
838 <https://doi.org/10.1029/2007GC001743>
- 839 Nadeau, R.M., & Dolenc, D. (2005), Nonvolcanic tremors deep beneath the San Andreas Fault.  
840 *Science* (80-. ). <https://doi.org/10.1126/science.1107142>
- 841 Nishikawa, T., Matsuzawa, T., Ohta, K., Uchida, N., Nishimura, T., & Ide, S. (2019), The slow  
842 earthquake spectrum in the Japan Trench illuminated by the S-net seafloor observatories.  
843 *Science* (80-. ). <https://doi.org/10.1126/science.aax5618>
- 844 Norris, R.J., & Cooper, A.F. (2001), Late Quaternary slip rates and slip partitioning on the  
845 Alpine Fault, New Zealand. *Journal of Structural Geology*. <https://doi.org/10.1016/S0191->

- 846 8141(00)00122-X
- 847 Obara, K. (2002), Nonvolcanic deep tremor associated with subduction in southwest Japan.  
848 *Science* (80- ). <https://doi.org/10.1126/science.1070378>
- 849 Obara, K. (2011), Characteristics and interactions between non-volcanic tremor and related slow  
850 earthquakes in the Nankai subduction zone, southwest Japan. *Journal of Geodynamics*.  
851 <https://doi.org/10.1016/j.jog.2011.04.002>
- 852 Obara, K., & Kato, A. (2016), Connecting slow earthquakes to huge earthquakes. *Science*.  
853 <https://doi.org/10.1126/science.aaf1512>
- 854 Panieri, G., Polonia, A., Lucchi, R.G., Zironi, S., Capotondi, L., Negri, A., & Torelli, L. (2013),  
855 Mud volcanoes along the inner deformation front of the Calabrian Arc accretionary wedge  
856 (Ionian Sea). *Marine Geology*. <https://doi.org/10.1016/j.margeo.2012.11.003>
- 857 Papadimitriou, E., Karakostas, V., Mesimeri, M., Chouliaras, G., & Kourouklas, C. (2017), The  
858 Mw6.5 17 November 2015 Lefkada (Greece) Earthquake: Structural Interpretation by  
859 Means of the Aftershock Analysis. *Pure and Applied Geophysics*.  
860 <https://doi.org/10.1007/s00024-017-1601-3>
- 861 Papazachos, B.C., & Papazachou, C. (2003), The Earthquakes of Greece. Ziti Publications,  
862 Thessaloniki (in Greek).
- 863 Peacock, S.M., & Wang, K. (1999), Seismic consequences of warm versus cool subduction  
864 metamorphism: Examples from southwest and northeast Japan. *Science* (80- ). 286, 937–  
865 939. <https://doi.org/10.1126/science.286.5441.937>
- 866 Peng, Z., & Chao, K. (2008), Non-volcanic tremor beneath the Central Range in Taiwan  
867 triggered by the 2001 Mw 7.8 Kunlun earthquake. *Geophysical Journal International*.  
868 <https://doi.org/10.1111/j.1365-246X.2008.03886.x>
- 869 Peng, Z., & Gomberg, J. (2010), An integrated perspective of the continuum between  
870 earthquakes and slow-slip phenomena. *Nature Geoscience*. <https://doi.org/10.1038/ngeo940>
- 871 Peng, Z., Gonzalez-Huizar, H., Chao, K., Aiken, C., Moreno, B., & Armstrong, G. (2013),  
872 Tectonic tremor beneath Cuba triggered by the Mw 8.8 maule and Mw 9.0 tohoku-oki  
873 earthquakes. *Bulletin of the Seismological Society of America*.  
874 <https://doi.org/10.1785/0120120253>
- 875 Peng, Z., Vidale, J.E., Wech, A.G., Nadeau, R.M., & Creager, K.C. (2009), Remote triggering of  
876 tremor along the San Andreas Fault in central California. *Journal of Geophysical Research:*  
877 *Solid Earth*. <https://doi.org/10.1029/2008JB006049>
- 878 Pérouse, E., Chamot-Rooke, N., Rabaute, A., Briole, P., Jouanne, F., Georgiev, I., & Dimitrov,  
879 D., (2012), Bridging onshore and offshore present-day kinematics of central and eastern  
880 Mediterranean: Implications for crustal dynamics and mantle flow. *Geochemistry,*  
881 *Geophysics and Geosystems*. <https://doi.org/10.1029/2012GC004289>

- 882 Pfohl, A., Warren, L.M., Sit, S., & Brudzinski, M. (2015), Search for tectonic tremor on the  
 883 central north Anatolian fault, Turkey. *Bulletin of the Seismological Society of America*.  
 884 <https://doi.org/10.1785/0120140312>
- 885 Rogers, G., & Dragert, H. (2003), Episodic tremor and slip on the Cascadia subduction zone:  
 886 The chatter of silent slip. *Science* (80- ). <https://doi.org/10.1126/science.1084783>
- 887 Romanet, P., Bhat, H.S., Jolivet, R., & Madariaga, R. (2018), Fast and Slow Slip Events Emerge  
 888 Due to Fault Geometrical Complexity. *Geophysical Research Letters*.  
 889 <https://doi.org/10.1029/2018GL077579>
- 890 Rousset, B., Jolivet, R., Simons, M., Lasserre, C., Riel, B., Milillo, P., Çakir, Z., & Renard, F.  
 891 (2016), An aseismic slip transient on the North Anatolian Fault. *Geophysical Research*  
 892 *Letters*. <https://doi.org/10.1002/2016GL068250>
- 893 Rubinstein, J.L., Vidale, J.E., Gomberg, J., Bodin, P., Creager, K.C., & Malone, S.D. (2007),  
 894 Non-volcanic tremor driven by large transient shear stresses. *Nature*.  
 895 <https://doi.org/10.1038/nature06017>
- 896 Ryan, W.B.F., Carbotte, S.M., Coplan, J.O., O'Hara, S., Melkonian, A., Arko, R., Weissel, R.A.,  
 897 Ferrini, V., Goodwillie, A., Nitsche, F., Bonczkowski, J., & Zemsky, R. (2009), Global  
 898 multi-resolution topography synthesis. *Geochemistry, Geophysics and Geosystems*.  
 899 <https://doi.org/10.1029/2008GC002332>
- 900 Saffer, D.M., & Wallace, L.M. (2015), The frictional, hydrologic, metamorphic and thermal  
 901 habitat of shallow slow earthquakes. *Nature Geoscience*. <https://doi.org/10.1038/ngeo2490>
- 902 Saltogianni, V., Mouslopoulou, V., Oncken, O., Nicol, A., Gianniou, M., & Mertikas, S. (2020),  
 903 Elastic fault interactions and earthquake-rupture along the southern Hellenic subduction  
 904 plate-interface zone in Greece. *Geophysical Research Letters*.  
 905 <https://doi.org/10.1029/2019GL086604>
- 906 Scholz, C.H. (1998), Earthquakes and friction laws. *Nature*. <https://doi.org/10.1038/34097>
- 907 Schwartz, S.Y., & Rokosky, J.M. (2007), Circum-Pacific Subduction Zones. *Reviews*  
 908 *Geophysics*. <https://doi.org/10.1029/2006RG000208.1>
- 909 Selvaggi, G., & Chiarabba, C. (1995), Seismicity and P-wave velocity image of the Southern  
 910 Tyrrhenian subduction zone. *Geophysical Journal International*.  
 911 <https://doi.org/10.1111/j.1365-246X.1995.tb06441.x>
- 912 Şengör, A.M., Tüysüz, O., İmren, C., Sakıncı, M., Eyidoğan, H., Görür, N., Le Pichon, X.,  
 913 Rangin, C. (2005), The North Anatolian Fault: A New Look. *Annual Reviews of Earth and*  
 914 *Planetary Science*. <https://doi.org/10.1146/annurev.earth.32.101802.120415>
- 915 Shelly, D.R., Beroza, G.C., & Ide, S. (2007), Non-volcanic tremor and low-frequency earthquake  
 916 swarms. *Nature*. <https://doi.org/10.1038/nature05666>
- 917 Shelly, D.R. (2017), A 15 year catalog of more than 1 million low-frequency earthquakes:

- 918 Tracking tremor and slip along the deep San Andreas Fault. *Journal of Geophysical*  
 919 *Research: Solid Earth*. <https://doi.org/10.1002/2017JB014047>
- 920 Sodoudi, F., Kind, R., Hatzfeld, D., Priestley, K., Hanka, W., Wylegalla, K., Stavrakakis, G.,  
 921 Vafidis, A., Harjes, H.P., & Bohnhoff, M. (2006), Lithospheric structure of the Aegean  
 922 obtained from P and S receiver functions. *Journal of Geophysical Research: Solid Earth*.  
 923 111. <https://doi.org/10.1029/2005JB003932>
- 924 Speranza, F., Minelli, L., Pignatelli, A., & Chiappini, M. (2012), The Ionian Sea: The oldest in  
 925 situ ocean fragment of the world? *Journal of Geophysical Research: Solid Earth*, 117, 1–13.  
 926 <https://doi.org/10.1029/2012JB009475>
- 927 Stein, R.S., Barka, A.A., & Dieterich, J.H. (1997), Progressive failure on the North Anatolian  
 928 fault since 1939 by earthquake stress triggering. *Geophysical Journal International*.  
 929 <https://doi.org/10.1111/j.1365-246X.1997.tb05321.x>
- 930 Sun, W.F., Peng, Z., Lin, C.H., & Chao, K. (2015), Detecting deep tectonic tremor in taiwan  
 931 with a dense array. *Bulletin of the Seismological Society of America*.  
 932 <https://doi.org/10.1785/0120140258>
- 933 Syracuse, E.M., van Keken, P.E., Abers, G.A., Suetsugu, D., Bina, C., Inoue, T., Wiens, D., &  
 934 Jellinek, M. (2010), The global range of subduction zone thermal models. *Physics of the*  
 935 *Earth and Planetary Interiors*, 183, 73–90. <https://doi.org/10.1016/j.pepi.2010.02.004>
- 936 Thomas, A.M., Nadeau, R.M., & Bürgmann, R. (2009), Tremor-tide correlations and near-  
 937 lithostatic pore pressure on the deep San Andreas fault. *Nature*.  
 938 <https://doi.org/10.1038/nature08654>
- 939 Thomson, S.N., Stöckhert, B., & Brix, M.R. (1999), Miocene high-pressure metamorphic rocks  
 940 of Crete, Greece: rapid exhumation by buoyant escape, in: Ring, U., Lister, G., Willet, S.,  
 941 Brandon, M. (Eds.), *Exhumation Processes: Normal Faulting, Ductile Flow, and Erosion*.  
 942 *Geological Society, London, Special Publications*, 154, 87–107.  
 943 <http://dx.doi.org/10.1144/GSL.SP.1999.154.01.04>
- 944 Tunç, B., Çaka, D., Irmak, T.S., Woith, H., Tunç, S., Barış, Ş., Özer, M.F., Lühr, B.G., Günther,  
 945 E., Grosser, H., & Zschau, J. (2011), The Armutlu Network: An investigation into the  
 946 seismotectonic setting of Armutlu-Yalova-Gemlik and the surrounding regions. *Annals of*  
 947 *Geophysics*. <https://doi.org/10.4401/ag-4877>
- 948 van Hinsbergen, D.J.J., van der Meer, D.G., Zachariasse, W.J., & Meulenkaamp, J.E. (2006),  
 949 Deformation of western Greece during Neogene clockwise rotation and collision with  
 950 Apulia. *International Journal of Earth Sciences*, 95, 463–490.  
 951 <https://doi.org/10.1007/s00531-005-0047-5>
- 952 van der Elst, N.J., Delorey, A.A., Shelly, D.R., & Johnson, P. A. (2016), Fortnightly modulation  
 953 of San Andreas tremor and low-frequency earthquakes. *Proceedings of the National*  
 954 *Academy of Sciences*, 113(31), 8601–8605. <https://doi.org/10.1073/pnas.1524316113>

- 955 van Keken, P.E., Hacker, B.R., Syracuse, E.M., & Abers, G.A. (2011), Subduction factory: 4.  
 956 Depth-dependent flux of H<sub>2</sub>O from subducting slabs worldwide. *Journal of Geophysical*  
 957 *Research: Solid Earth*, 116. <https://doi.org/10.1029/2010JB007922>
- 958 Vernant, P., Reilinger, R., & McClusky, S. (2014), Geodetic evidence for low coupling on the  
 959 Hellenic subduction plate interface. *Earth and Planetary Science Letters*, 385, 122–129.  
 960 <https://doi.org/10.1016/j.epsl.2013.10.018>
- 961 Wallace, L.M., Beavan, J., Bannister, S., & Williams, C. (2012), Simultaneous long-term and  
 962 short-term slow slip events at the Hikurangi subduction margin, New Zealand: Implications  
 963 for processes that control slow slip event occurrence, duration, and migration. *Journal of*  
 964 *Geophysical Research Solid Earth*. <https://doi.org/10.1029/2012JB009489>
- 965 Walter, J.I., Schwartz, S.Y., Protti, J.M., & Gonzalez, V. (2011), Persistent tremor within the  
 966 northern Costa Rica seismogenic zone. *Geophysical Research Letters*.  
 967 <https://doi.org/10.1029/2010GL045586>
- 968 Walter, J.I., Schwartz, S.Y., Protti, M., & Gonzalez, V. (2013), The synchronous occurrence of  
 969 shallow tremor and very low frequency earthquakes offshore of the Nicoya Peninsula, Costa  
 970 Rica. *Geophysical Research Letters*. <https://doi.org/10.1002/grl.50213>
- 971 Wech, A.G. (2016), Extending Alaska's plate boundary: Tectonic tremor generated by Yakutat  
 972 subduction. *Geology*. <https://doi.org/10.1130/G37817.1>
- 973 Wech, A.G., Boese, C.M., Stern, T.A., & Townend, J. (2012), Tectonic tremor and deep slow  
 974 slip on the Alpine Fault. *Geophysical Research Letters*.  
 975 <https://doi.org/10.1029/2012GL051751>
- 976 Wech, A.G., & Creager, K.C. (2008), Automated detection and location of Cascadia tremor.  
 977 *Geophysical Research Letters*. <https://doi.org/10.1029/2008GL035458>
- 978 Wessel, P., Smith, W.H.F., Scharroo, R., Luis, J., & Wobbe, F. (2013), Generic mapping tools:  
 979 Improved version released. Eos (Washington, DC). <https://doi.org/10.1002/2013EO450001>
- 980 Wollin, C., Bohnhoff, M., Martínez-Garzón, P., Küperkoch, L., & Raub, C. (2018), A unified  
 981 earthquake catalogue for the Sea of Marmara Region, Turkey, based on automatized phase  
 982 picking and travel-time inversion: Seismotectonic implications. *Tectonophysics*.  
 983 <https://doi.org/10.1016/j.tecto.2018.05.020>
- 984 Yabe, S., Ide, S., & Yoshioka, S. (2014), Along-strike variations in temperature and tectonic  
 985 tremor activity along the hikurangi subduction zone, New Zealand. *Earth, Planets and*  
 986 *Space*. <https://doi.org/10.1186/s40623-014-0142-6>
- 987 Yang, H., & Peng, Z. (2013), Lack of additional triggered tectonic tremor around the Simi  
 988 Valley and the San Gabriel Mountain in southern California. *Bulletin of the Seismological*  
 989 *Society of America*. <https://doi.org/10.1785/0120130117>
- 990 Zor, E., Özalaybey, S., & Gürbüz, C. (2006), The crustal structure of the eastern Marmara  
 991 region, Turkey by teleseismic receiver functions. *Geophysical Journal International*.

992 <https://doi.org/10.1111/j.1365-246X.2006.03042.x>

993

994 **Supporting References**

995 Horstmann, T., Harrington, R. M., & Cochran, E. S. (2013), Semiautomated tremor detection  
996 using a combined cross-correlation and neural network approach. *Journal of Geophysical*  
997 *Research: Solid Earth*, 118(9), 4827-4846. <https://doi.org/10.1002/jgrb.50345>

998 Karabulut, H., Schmittbuhl, J., Özalaybey, S., Lengliné, O., Kömeç-Mutlu, A., Durand, V.,  
999 Bouchon, M., Daniel, G., & Bouin, M.P. (2011), Evolution of the seismicity in the eastern  
1000 Marmara Sea a decade before and after the 17 August 1999 Izmit earthquake.  
1001 *Tectonophysics*. <https://doi.org/10.1016/j.tecto.2011.07.009>

1002 Kassaras, I., Kapetanidis, V., & Karakonstantis, A. (2016), On the spatial distribution of  
1003 seismicity and the 3D tectonic stress field in western Greece. *Physics and Chemistry of the*  
1004 *Earth*. <https://doi.org/10.1016/j.pce.2016.03.012>